REVIEWS OF TOPICAL PROBLEMS

Specific features of spin, charge, and orbital ordering in cobaltites

Physics – Uspekhi **52** (8) 789 – 810 (2009)

REVIEWS OF TOPICAL PROBLEMS PACS numbers: **71.30.+h**, 75.30.Cr, 75.50.Pp

Specific features of spin, charge, and orbital ordering in cobaltites

N B Ivanova, S G Ovchinnikov, M M Korshunov, I M Eremin, N V Kazak

DOI: 10.3367/UFNe.0179.200908b.0837

Contents

Abstract. Complex cobalt oxides known as cobaltites are reviewed, including $Ln CoO_3$-based perovskite-structured rare-earth cobaltites (where *Ln* is lanthanum or a lanthanide), quasi-two-dimensional and quasi-one-dimensional cobaltites of the types $Ln Co_2O_{5+\delta}$, La_2CoO_4, and $Ca_3Co_2O_8$, and $Na_xCoO_2 \cdot yH_2O$ superconducting compounds. Key experimental and theoretical results are presented, with emphasis on the interplay between charge, spin, and orbital degrees of freedom. Two problems of specific relevance to cobaltites — the spin state instability of Co^{3+} ions in $Ln CoO_3$, and the nature of superconductivity in $Na_xCoO_2 \cdot yH_2O$ — are also given significant attention.

N B Ivanova Siberian Federal University,
ul. Kirenskogo 26, 660074 Krasnoyarsk, Russian Federation
Tel. (7-391) 249 75 89. Fax (7-391) 243 06 92. E-mail: adm@kgtunnet.ru
S G Ovchinnikov Siberian Federal University,
ul. Kirenskogo 26, 660074 Krasnoyarsk, Russian Federation
Tel. (7-391) 249 75 89. Fax (7-391) 243 06 92. E-mail: adm@kgtunnet.ru
Kirensky Institute of Physics,
Siberian Branch of the Russian Academy of Sciences,
Akademgorodok 50-38, 660036 Krasnoyarsk, Russian Federation
Tel. (7-391) 249 45 59. Fax (7-391) 243 89 23. E-mail: dir@iph.krasn.ru
M M Korshunov Kirensky Institute of Physics,
Siberian Branch of the Russian Academy of Sciences,
Akademgorodok 50-38, 660036 Krasnoyarsk, Russian Federation
Tel. (7-391) 249 45 59. Fax (7-391) 243 89 23. E-mail: dir@iph.krasn.ru
Max-Planck-Institut für Physik Komplexer Systeme,
Nöthnitzer Straße 38, D-01187 Dresden, Germany
Tel. (49) 351-8710. Fax (49) 351 871-1999
E-mail: info@mpipks-dresden.mpg.de
I M Eremin Max-Planck-Institut für Physik Komplexer Systeme,
Nöthnitzer Straße 38, D-01187 Dresden, Germany
Tel. (49) 351-8710. Fax (49) 351 871-1999
E-mail: info@mpipks-dresden.mpg.de
Kazan State University,
ul. Kremlevskaya 18, 420008 Kazan, Russian Federation
Tel. (7-843) 292 69 77. Fax (7-843) 292 44 48. E-mail: public.mail@ksu.ru
N V Kazak Kirensky Institute of Physics,
Siberian Branch of the Russian Academy of Sciences,
Akademgorodok 50-38, 660036 Krasnoyarsk, Russian Federation
Tel. (7-391) 249 45 59. Fax (7-391) 243 89 23. E-mail: dir@iph.krasn.ru

Received 3 April 2009
Uspekhi Fizicheskikh Nauk **179** (8) 837 – 860 (2009)
DOI: 10.3367/UFNr.0179.200908b.0837
Translated by V I Kisin; edited by A M Semikhatov

1. Introduction

The discovery of high-temperature superconductivity in layered cuprates stimulated tremendous interest in other perovskite-structured oxides of 3d metals; these compounds have been thoroughly investigated in the last two decades. The feature common to most of them is that they belong to systems with strong electron correlations (SECs) [1], which result in the dielectric ground state of undoped La_2CuO_4 cuprates, $LaMnO_3$ manganites, and $LaCoO_3$ cobaltites. Doping in cuprates produces an unusual pseudogap state and high-temperature superconductivity (see, e.g., reviews [2–5]). In manganites, doping leads to competition of the antiferromagnetic and ferromagnetic exchange interactions and to colossal magnetoresistance [6–9]. In ruthenates, we observe exotic superconductivity in the case of Sr_2RuO_4 and metal–dielectric transitions in the system $Ca_{2-x}Sr_xRuO_4$ [10, 11]. The natural question now is: what is so new and special that studies of cobaltite could give to a wide range of *Physics–Uspekhi* readers and is there a need at all for a special review on cobaltites? We think that this need does exist, for the following reasons.

First, in cobaltites, we find all the phenomena known in cuprates and manganites: dielectric–metal transitions, super-

conductivity [12], competition of antiferromagnetic and ferromagnetic exchanges, giant magnetoresistance [13, 14], and anomalously high thermo-emf [1, 15, 16]. It is likely that the study of superconductivity in $Na_xCoO_2 \cdot yH_2O$ layered cobaltites will allow extracting additional data on the nature of high-temperature superconductivity (HTSC) in cuprates. At the same time, the exotic superconductivity in these cobaltites is of interest in itself because it arises on a triangular lattice of cobalt ions where considerable frustration effects are possible.

Second, the interrelation between spin and orbital degrees of freedom is very strongly pronounced in cobaltites. Orbital ordering is also well known in manganites, but changes in the orbital and spin states of the Co^{3+} ion in cobaltites manifest themselves in the competition between the low-spin (LS) t_{2g}^6, $S = 0$, high-spin (HS) $t_{2g}^4 e_g^2$, $S = 2$, and intermediate-spin (IS), $t_{2g}^5 e_g^1$, $S = 1$ levels. This competition is responsible for the specific features of the magnetic, electric, and structural properties of rare-earth cobaltites $LaCoO_3$. High spin–orbital degeneration is regarded as a possible cause of giant magnetostriction [17] and of the considerable thermoelectric effects [15, 16] that appear attractive from the standpoint of applications.

Third, cobaltites have proved to be a windfall for demonstrating the advantages of unique new experimental techniques for studying magnetic materials developed over the last 10–15 years, such as the X-ray magnetooptics using synchrotron sources (see review [18]). Examples of separating the orbital and spin contributions to the magnetic moments of $LaCoO_3$ and $Ca_3Co_2O_8$ using X-ray magnetic circular dichroism and applying this information for clarifying the state, spin, and orbital states are given in the present review.

Cobaltites thus demonstrate a very rich collection of properties, some of which belong exclusively to them. SEC effects so typical of 3d elements are definitely present in cobaltites, and this both creates additional complications for the theory and enriches the physics of the phenomena.

2. Perovskite-structured cobaltites

2.1 Crystalline structure and physical properties of rare-earth *Ln*CoO_3 cobaltites

The class of rare-earth cobaltites includes several families; the best studied among them are compounds with the general formula *Ln*CoO_3, where *Ln* stands for lanthanum, yttrium, or a lanthanide (Pr, Nd, Sm, Eu, Gd, Tb...). The basic representative of this series is $LaCoO_3$, whose valence formula is $La^{3+}Co^{3+}O_3^{2-}$. Both transition and rare-earth elements manifest the same valence, 3. It was shown in one of the earliest papers that treated the crystalline structure of these compounds in detail [19] that at room temperature, $LaCoO_3$ has a rhombohedrally distorted perovskite-structured lattice whose unit cell belongs to the spatial group $R\bar{3}c$, D_{3d}^6 (Fig. 1a).

The crystalline lattice of all other compounds of the *Ln*CoO_3 series with *Ln* = Y, Pr, Sm, Eu, Gd... contains rhombic distortions, the spatial group being *Pbnm*, V_h^{16} (Fig. 1b) [19]. The extent of distortion differs for different kinds of *Ln* ions. The lowest distortion is found in $NdCoO_3$, with an almost cubic structure. Therefore, cobalt ions in the *Ln*CoO_3 compounds are surrounded by weakly distorted oxygen octahedra and form CoO_6 complexes.

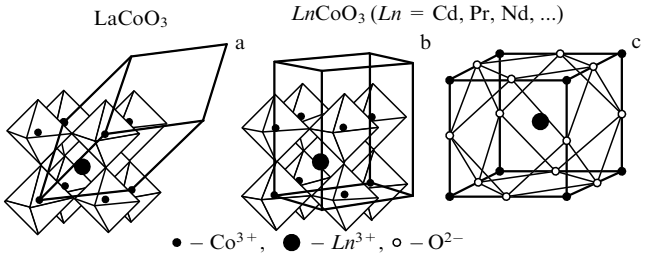

Figure 1. Perovskite-type crystalline structure of *Ln*CoO_3 (a) with rhombohedral distortions, group $R\bar{3}c$ ($LaCoO_3$), (b) with rhombohedral distortions, group *Pbnm* (*Ln*CoO_3 with *Ln* ≠ La) [19], (c) surroundings of a rare-earth ion [20].

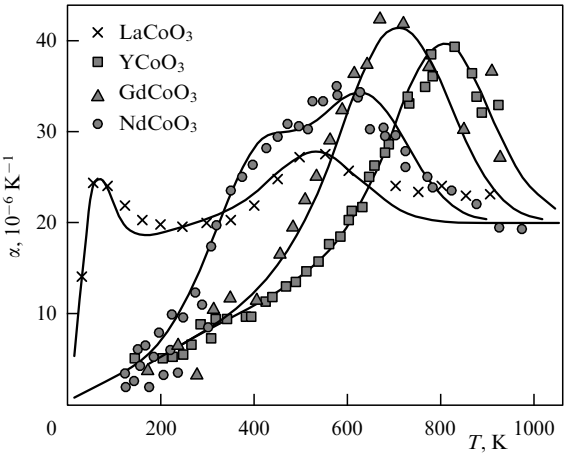

Figure 2. Curves of the linear thermal expansion coefficient α of a crystal lattice as a function of temperature [22].

Only one type of position exists for the ion of a transition element in stoichiometric compounds. However, rare-earth cobaltites are typically somewhat deficient in oxygen. We note that part of the cobalt ions are surrounded not by octahedral but by pyramidal complexes. The pyramidal surroundings of cobalt ions are also typical of layered compounds of the $LnMCo_2O_{5+\delta}$ series (*M* stands for alkaline-earth elements).

The surroundings of a rare-earth ion in *Ln*CoO_3 has the lower symmetry C_s. The trivalent rare-earth ion Ln^{3+} is surrounded by a somewhat distorted cubo-octahedron (Fig. 1c) formed of 12 oxygen ions with which the rare-earth ion forms three long bonds, six medium-length bonds, and three short bonds. As the number of lanthanides in the group increases, the unit cell volume decreases linearly as a result of a decrease in the ionic radius of the rare-earth element [20, 21].

The extent of structural distortion in *Ln*CoO_3 changes with temperature appreciably and, as a rule, nonmonotonically [22]. Anomalous thermal expansion of rare-earth cobaltites is a striking feature of their behavior. According to the data in [22] and subsequent paper [23], the linear thermal expansion coefficient of *Ln*CoO_3 (where *Ln* = La, Dy, Sm, Pr, Y, Gd, or Nd) is a nonmonotonic function of temperature and displays maxima whose positions correlate with the specifics of magnetic susceptibility and conductivity (Fig. 2).

In fact, the compound $LaCoO_3$ first attracted attention precisely because of the unusual temperature dependence of

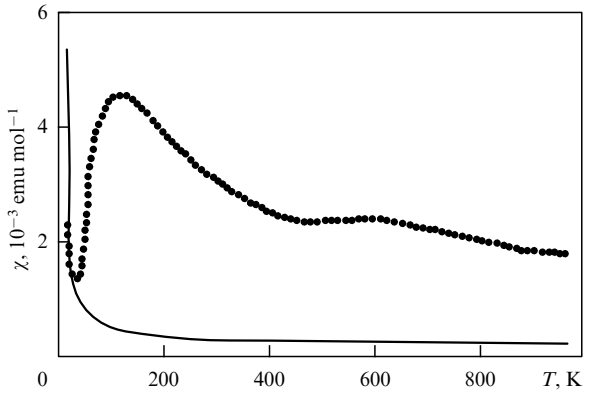

Figure 3. Temperature dependence of the magnetic susceptibility of $LaCoO_3$ [25]. The solid curve plots the contribution of magnetic impurities (emu denotes the electromagnetic unit).

Table 1. Ionic radii of the Co^{3+} ion in different spin states.

State	Spin	r, Å
LS	0	0.545
IS	1	0.560
HS	2	0.610

its magnetic susceptibility $\chi(T)$ [24, 25], which has two broad maxima at $T_1 \approx 100$ K and $T_2 \approx 500$ K. At high temperatures, the susceptibility slowly decreases as the temperature increases (Fig. 3). A study of polarized neutron scattering [26] and the Knight shift in $LaCoO_3$ [27] showed that the cobalt ions are in a low-spin nonmagnetic state at low temperatures, but this state becomes paramagnetic at temperatures above 100 K. Cobalt ions have different ionic radii r in different spin states (see Table 1).

A change in the spin state is accompanied by a corresponding change in the volume of the unit cell. No long-range magnetic ordering was found in $LaCoO_3$.

In other compounds of the $LnCoO_3$ series, the same specific features are observed in the magnetic susceptibility χ and thermal expansion as in $LaCoO_3$; however, two anomalies in $\chi(T)$ are less separated from each other in temperature, are not as well defined, and are shifted to a higher temperature range. Neutron scattering data [28, 29] showed no spin transitions at temperatures up to room temperature for compounds with Ln = Pr, Nd, Sm, Eu. In $Ho_{1-x}Ca_xCoO_3$, there is no transition to another spin state at temperatures up to 900 K [30]. The temperatures of spin transitions are in each case higher than the spin transition temperature for $LaCoO_3$ (100 K). Structural anomalies accompanying the magnetic transition in the compounds $LnCoO_3$ (Ln = Y, Sm, Dy, Gd) are also observed at temperatures that are considerably higher than room temperature [22]. Three ranges can be identified in the phase diagram of the $LnCoO_3$ series with rare-earth ions from La to Lu (Fig. 4): nonmagnetic dielectric, paramagnetic dielectric, and paramagnetic metal [31]. Transitions between them are smooth and spread out, because these are not phase transitions in the classical sense of the term but crossovers.

The transition between different spin states in $LaCoO_3$ can be stimulated not only by applying temperature but also by applying external pressure [32, 33] and illuminating with light [34]. A compression of the crystal lattice and a reduction of the Co–O bond length stabilizes the nonmagnetic state of the Co^{3+} ion regardless of the way this was achieved.

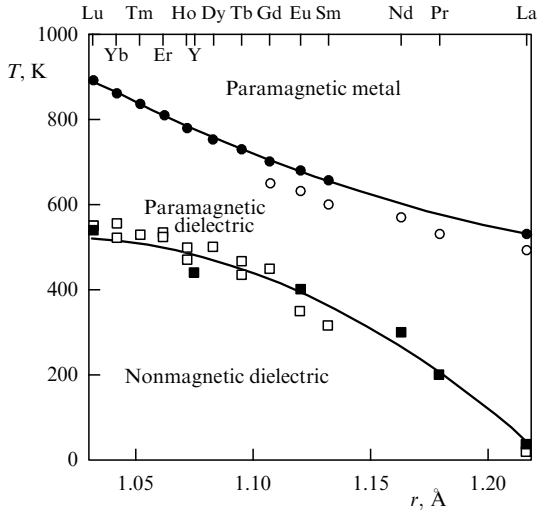

Figure 4. Electron phase transition of compounds of the $LnCoO_3$ series, in $r-T$ coordinates (r is the ionic radius) [31].

The dielectric properties of compounds are also affected by transitions between different spin states of Co^{3+} as the ion radii vary from state to state. The real and imaginary parts of the dielectric permittivity of single crystals of $LnCoO_3$ (Ln = La, Pr, Gd) change sharply with increasing the temperature; specific features of the temperature dependence of the dielectric permittivity measured at low frequencies (5–10 kHz) are not very different from the behavior of the static magnetic susceptibility and thermal expansion [35]. The authors of Ref. [35] point to a similarity in the dielectric permittivity as a function of temperature and frequency for cobaltites and ferroelectric relaxors and conclude that $LaCoO_3$ is in an inhomogeneous state in which the paramagnetic monoclynic phase coexists with the nonmagnetic rhombohedral phase. Evidence of inhomogeneity is also suggested by the data of X-ray absorption spectra [36], which are discussed in Section 2.2.

As a rule, the electric resistance of cobaltites substantially increases as the temperature decreases, but the type of temperature dependence and the effect of the magnetic state depend greatly on the composition. In the case of $LaCoO_3$, only a very weak anomaly of resistance against the background of smooth change accompanies the low-temperature anomaly of magnetic susceptibility in the vicinity of the 100 K point. The activation energy is almost constant in this region and approximately equals 0.2 eV [37]. In contrast to this, the high-temperature anomaly is accompanied by a smooth semiconductor–metal transition, which is evidence of delocalization of charge carriers. We note that a considerable decrease in resistance is also observed in the temperature range above 500 K. In view of this, the high-temperature anomaly of magnetic susceptibility is usually treated in the current literature as having a 'nonmagnetic nature.' Similar transitions in conductivity are also typical for other representatives of the family of pseudocubic rare-earth cobaltites [38], except that they, along with magnetic susceptibility anomalies, are observed at a higher temperature than in $LaCoO_3$.

The temperature dependence of electric conduction in rare-earth-cobaltites does not obey a simple activation law.

The activation energy of conductivity at a point, defined as the derivative of the logarithm of conduction with respect to the inverse temperature, changes with temperature in a wide range of undoped $LnCoO_3$ compounds nonmonotonically and has a maximum whose position on the temperature axis correlates with the maximum linear thermal expansion of the lattice and with a high-temperature transition in the magnetic susceptibility [22]. At low temperatures, the Mott hopping conductivity is typical for many compounds with cobalt oxides [39, 40].

The nature of the dielectric–metal transition in $LaCoO_3$ occurring as the temperature increases has been discussed in various contexts: as thermal population of e_g states accompanying the lengthening of the Co–O bond [41], as narrowing of the semiconducting gap between unoccupied e_g states and filled t_{2g} states [42], or as an order–disorder transition in the case of orbital ordering [43]. A comparison of data on ordinary and optical conduction jointly with Hall measurements in [37] showed that the conventional scenario of a collapsing dielectric gap does not work for rare-earth cobaltites. High-temperature transport measurements confirmed that at $T > 400$ K, the charge gap width rapidly decreases as the temperature increases, and a metal-type state, not a semimetal one, characterized by a large Fermi surface, is formed at $T \approx 800$ K. After the spin transition is completed, all observable properties of the thermally induced metal–insulator transition (MIT) are typical of the Mott transition in strongly correlated electron systems.

2.2 Electron structure, spin, and orbital moment in $LnCoO_3$

Similarly to the situation in the physics of perovskite-structured cuprates, the key problem is the mechanism of high-temperature superconductivity, and in manganites, the nature of the colossal magnetic susceptibility; in rare-earth-cobaltites, a similar role is played by the problems of transitions between high-spin, low-spin, and intermediate-spin states of the cobalt ion. We know that in the octahedral crystal field, the initially fivefold degenerate 3d level of the Co^{3+} ion splits into triply degenerate t_{2g} orbitals and doubly degenerate e_g orbitals. The amount of degeneration is $\Delta = 10\,Dq$, where $10\,Dq$ is the parameter of the crystal field. By Hund's rule, the electron configuration d^6 must correspond to the HS state $t_{2g}^4 e_g^2$ with the spin $S = 2$, but as the crystal field increases, an HS–LS crossover occurs [44] in which the LS state has the t_{2g}^6 configuration. For any parameters realistic for $LnCoO_3$, the critical value of Δ in the purely ionic Tanabe–Sugano model is $\Delta \approx 2$ eV [36, 45].

Numerous experiments conducted with $LaCoO_3$ and related compounds showed that the nonmagnetic (LS) state is realized at low temperatures in all compounds of the $LnCoO_3$ series. It is also clear from the entire set of experimental data that the spin transition in $LaCoO_3$ at $T \approx 100$ K corresponds to the increasing magnetic moment of Co^{3+}. The presence of the HS–LS crossover on the Tanabe–Sugano diagram is a sign that the crystal field Δ in $LnCoO_3$ may be close to the critical value Δ_c. If $\Delta > \Delta_c$, then the LS is the ground level and the HS is the nearest excited level. Precisely this model was proposed half a century ago in [46]; in it, the low-temperature susceptibility anomaly corresponds to the thermally activated spin transition from the LS to the HS state. When the ratio of the numbers of ions in the LS and HS states reaches 1:1, a magnetic superstructure is formed in which these ions alternate. The existence region of the superstructure corresponds to a susceptibility plateau between the two transitions. According to [46], the second anomaly stems from the semiconductor–metal transition, destruction of magnetic superstructure, transition of all the cobalt to the HS state, and realization of ordinary paramagnetism. In many early studies [46], the temperature transition in the vicinity of $T = 100$ K was interpreted as thermal population of the excited HS state from the ground LS state [47–49]. But in most of the later studies (mostly X-ray and neutron scattering), no signs of formation of a magnetic superstructure in $LaCoO_3$ were detected. Nevertheless, we note that the possibility of the formation of superstructures in the presence of transition ions in various spin states is discussed theoretically in [50] and such spin superstructures were indeed discovered in $TlSr_2CoO_5$ and in other layered cobaltites [51, 52]. Magnetic data also disagree with the assumption of the LS–HS crossover; namely, attempts to describe $\chi(T)$ by the Curie law at $T > 100$ K give the spin value S closer to 1 than to 2.

In order to remove the accumulating contradictions, a two-stage model was suggested in [53, 54] in which the first anomaly in susceptibility at $T = 100$ K was interpreted as a transition from the low-spin state to an intermediate-spin state (LS $\rightarrow$ IS), and the second as a transition from IS to HS. The presence of Co^{3+} ions in the high-spin state at $T > 500$ K is confirmed by experimental studies of electric conduction [55], photoemission [56], thermal expansion [57], and specific heat capacity [58]. As regards the intermediate temperature range 100–500 K, numerous and quite advanced studies have so far failed to produce any unambiguous evidence in favor of the realization of the IS or HS state. For instance, recent experiments on the spectroscopy of electron losses have unambiguously (in the opinion of the authors of [59]) refuted the hypothesis of the HS state of Co ions in $LaCoO_3$. The IS scenario is also supported by the Jahn–Teller distortion of the crystal lattice and Jahn–Teller polarons discovered in [60, 61]. Nevertheless, the latest studies of the local structure of $LaCoO_3$ [62] have failed to detect any appreciable Jahn–Teller distortions or reduction in symmetry to the group $I2/a$ that was reported earlier in [60]. A number of other data (electron paramagnetic resonance (EPR), X-ray spectroscopy, and X-ray circular dichroism [36, 63, 64]) also support the hypothesis of the HS state.

As regards the theoretical aspect of the problem, the wide popularity of the two-stage model including the IS state of Co ions is due to theoretical paper [43], which showed, using the local density approximation (LDA) and taking account of the Coulomb interaction (LDA + U), that the IS state can be stabilized through the effects of hybridization of the Co-3d and O-2p orbitals. The factor that plays an important role here is the orbital ordering of the IS state, which is schematically shown in Fig. 5. Two different orbital configurations are ordered in the model proposed in [43]. Position *1* in Fig. 5 shows an ion with a filled $d_{y^2-z^2}e_g$ orbital, and the ion in position *2* has the $d_{x^2-z^2}$ orbital filled. Recent calculations of the electron structure of $LaCoO_3$ and $PrCoO_3$ [65, 66] by the generalized gradient approximation (GGA) method with the spin–orbit interaction taken into account (GGA + U) extended the scenario suggested in [43]. The authors of [65, 66] calculated the electron structure at finite temperatures with lattice parameters taken from experimental data for the given temperature. Figure 6a clearly shows a peak near the Fermi level formed by the three-dimensional states of cobalt in the LS configuration. The spin–orbit interaction does not modify

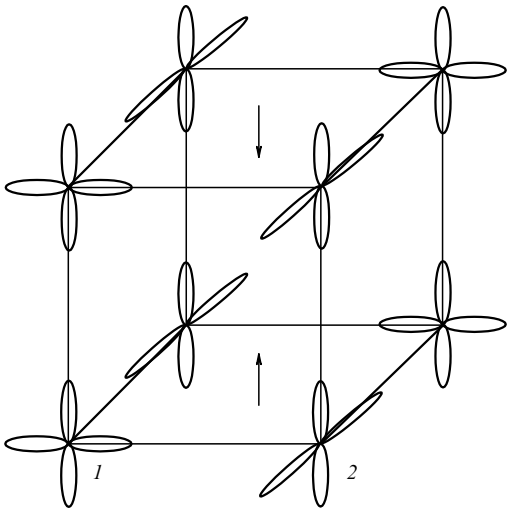

Figure 5. Hypothetical orbital ordering in $LaCoO_3$ [43]. Arrows indicate the orientation of spins.

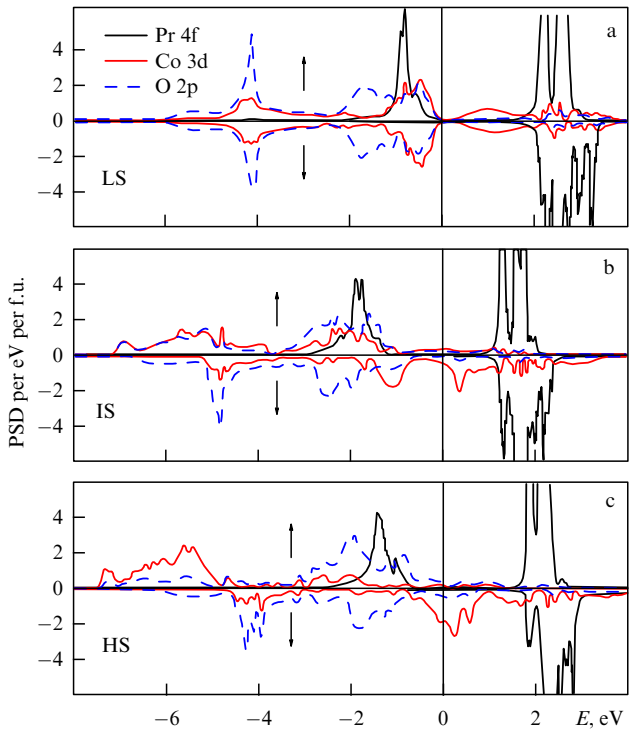

Figure 6. Partial state densities (PSDs) of Pr-4f, Co-3d, and O-2p corresponding to the configurations LS (a), IS (b), and HS (c) and calculated by the GGA + U method taking the spin–orbit coupling into account [66] (f.u.: formula unit).

these LS states; for the IS state, it splits the peak due to 3d electrons of Co into two peaks, one below and one above the Fermi level. For the HS state, the spin–orbit interaction shifts this peak into the region above the Fermi level. A comparison of the results with the experimental spectra of photoelectrons originating from the valence band shows good agreement at room temperature for the IS state both in $LaCoO_3$ and in $PrCoO_3$ (Fig. 7). As the temperature decreases, the contribution of the low-spin state increases such that the temperature dependence of the absorption edge in [66] is found to be in good agreement with the temperature

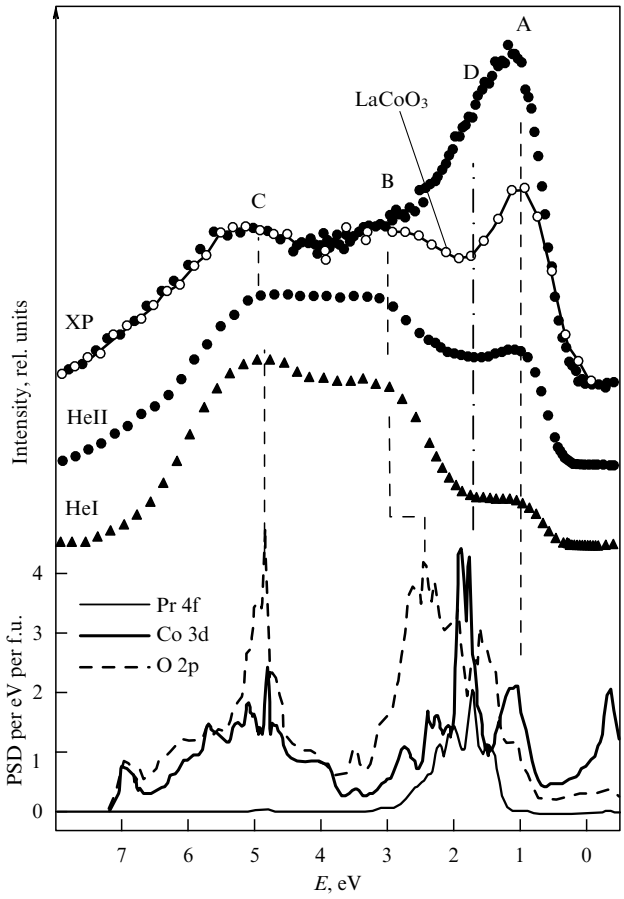

Figure 7. The structure of the experimentally determined valence band of $PrCoO_3$ using the data of X-ray photoemission (XP) and HeI- and HeII-radiation spectroscopy at room temperature. Only the XP spectrum is plotted for $LaCoO_3$. The lower part of the figure shows the PSDs corresponding to the IS state of the cobalt ion, calculated by the GGA + U method taking the spin–orbit coupling into account [66].

dependence of the dielectric gap determined from the conductivity data. In LDA + U and GGA + U calculations, however, the assumption is that electron energy states split according to spin, which can be acceptable only in magnetically ordered substances. No long-range magnetic ordering was found in $LaCoO_3$, and hence the proofs of IS stabilization based on LDA + U and GGA + U calculations can hardly be considered credible.

We consider the diagram of the formation of the electron structure of $LaCoO_3$ in detail, taking the SEC effects into account. The kinetic energy of electrons in a Mott–Hubbard insulator is small compared with their potential energy. If we completely neglect the kinetic energy, we arrive at an assembly of Co^{3+} ions in a cubic crystal field (the possible small distortions of the crystal field due to deformations of the CoO_6 octahedron can be additionally taken into account later). We know that jointly taking the intra-atomic Coulomb interaction and the crystal field into account leads to the Tanabe–Sugano diagram of multielectron configurations (Fig. 8) (levels d^6 in the case of Co^{3+}) [44]. This diagram is best described for $LaCoO_3$ in a series of papers [45, 67, 68]. As the crystal field increases, the crossover of HS–LS states occurs (see Fig. 8); consequently, the results depend on the parameters rather strongly. For instance, an early paper [67] assumed that the ground level of Co^{3+} is the high-spin one (in

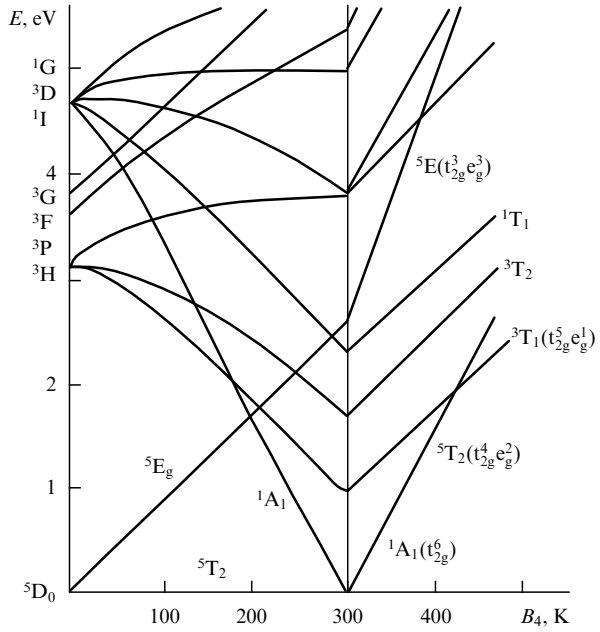

Figure 8. Energy of electron levels of the Co^{3+} ion as a function of the crystal field (the Tanabe–Sugano diagram) [44]. B_4 is the Racah parameter for an octahedral crystal field.

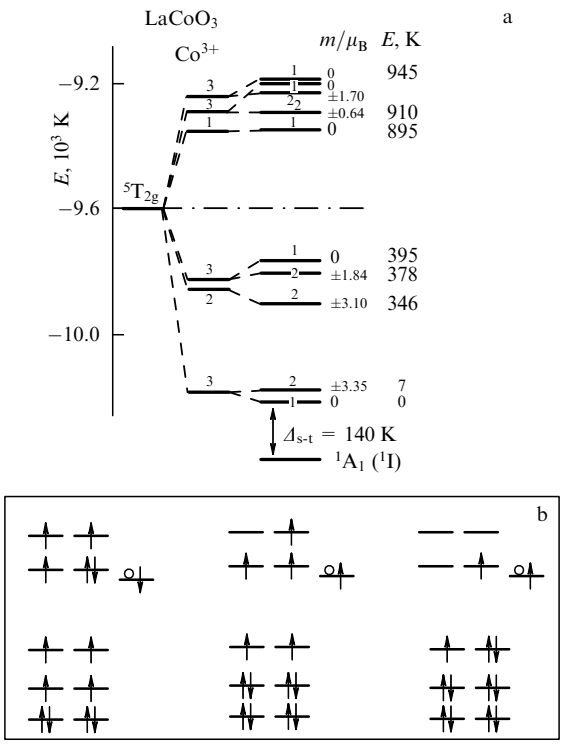

Figure 9. (a) Electron structure of Co^{3+} in the ionic model of $LaCoO_3$ [67], where Δ_{s-t} is the energy of activation of the singlet–triplet transition. (b) Diagram of the electron configuration $d^6 + d^7\underline{L}$: high-spin, intermediate-spin, and low-spin states.

the limit $\Delta \to 0$, this is the atomic ^5D energy level). The crystal field and the spin–orbit interaction split it into three sublevels with the effective moments $\tilde{J} = 1$, 2, and 3 (Fig. 9a); we note that the lower triplet is split into the levels $|0\rangle$ and $|\pm 1\rangle$ by the trigonal component of the crystal field. In Ref. [67], it was assumed that each Co^{3+} ion at $T = 0$ is in the nonmagnetic state $|0\rangle$ and the doublet $|\pm 1\rangle$ is populated gradually as the temperature increases. But EPR measurements [63] disproved this theory and showed that the resonance is observed with transitions not from the ground level but from the excited level of the triplet. The intensity of the EPR signal depends on temperature in the activation-energy manner:

$$I(T) = I_0 \exp\left(-\frac{E_0}{T}\right)$$

with the activation energy $E_0 = 140$ K [63]. In subsequent paper [68], the authors therefore assumed that the crystal field in $LaCoO_3$ is $\Delta \geqslant \Delta_c$ (Δ_c is the crossover field). Then the ground level at $T = 0$ is the low-spin singlet $^1A_1$ shown in the lower part of Fig. 9a; the singlet is separated by the gap $\Delta_{s-t} = E_0 = 140$ K from the triplet sublevel $|0\rangle$. With this arrangement, it was possible to successfully describe the EPR spectra and to fine-tune the parameters such that the g-factor coincided with the experimentally observed value. The authors of Refs [67, 68] made the following important general conclusion: the orbital moment in $LaCoO_3$ is 'unfrozen,' in contrast to the orbital moment in the familiar picture of spin magnetism in oxides of 3d metals. It must be remembered, however, that the purely ionic picture exists only in the zeroth approximation in interatomic hopping, resulting in a covalent admixture of d^7p^5 states to ionic d^6p^6 states (the spectroscopic notation d^6 for the ionic state and $d^7\underline{L}$ for the state with a hole on the ligand, is frequently encountered in the literature, e.g., in [56]).

To take the covalence of Mott–Hubbard insulators into account, a widespread method of configurational interaction in the cluster model that covers all atomic multiplets and hybridization with the p-states of the ligand (oxygen for the CoO_6 cluster) is used [69, 70]. The diagram of the $d^6 + d^7\underline{L}$ configurations of the Co^{3+} ion for HS, IS, and LS states is shown in Fig. 9b. A similar calculation for $LaCoO_3$ and the determination of the parameters of the model by comparing them with the experimental results of X-ray absorption spectra (XAS) and X-ray magnetic circular dichroism (XMCD) are described in [36]. We note that the dichroism signal is the difference between absorption spectra with two opposite polarizations and is therefore small, about 1% of the XAS signal in [36]; however, the high energy resolution (relative resolving power of several meV) allowed reliably measuring the XMCD signal. The sum rule in [71] was used to separate the orbital moment L_z from the spin moment S_z and calculate the ratio $L_z/S_z \approx 0.5$ [36]. The results of calculating the levels by the method of configurational interaction (essentially an analog of the Tanabe–Sugano diagrams for multielectron molecular orbitals of the CoO_6 cluster) show that as the crystal field increases, the HS – LS crossover occurs as in the ionic model. However, owing to the covalent admixture, the wave function of the ground state of the CoO_6 cluster then takes the form [72]

$$\Psi = \alpha_6|d^6\rangle + \alpha_7|d^7\underline{L}\rangle + \alpha_8|d^8\underline{L}^2\rangle + \alpha_9|d^9\underline{L}^3\rangle\,,$$

$$|\alpha_6|^2 + |\alpha_7|^2 + |\alpha_8|^2 + |\alpha_9|^2 = 1\,.$$

The ground state corresponds to LS and the first excited level (split by the spin–orbit interaction to sublevels with the effective moment $J = 1, 2, 3, \ldots$, as also in [68]) corresponds

to HS. But because of the covalent mixing $J = 1$, the triplet is characterized by $\langle L_z \rangle \approx 0.6$ and $\langle S_z \rangle \approx 1.3$ with the L_z/S_z ratio not very different from the experimental value 0.5. At the same time, $\langle S^2 \rangle$ is close to 6 and the g factor equals 3.2 (the experimental EPR value is $g = 3.35$ [63]). The authors believe that the closeness of $\langle S_z \rangle$ to 1 may be the reason why the point of view is so widespread that IS states make the leading contribution to the spin transition in $LaCoO_3$ at the temperature 100 K.

We also note that the authors of [36] succeeded in describing the XAS spectra at different temperatures only after assuming that the LS state has the parameter $10\,Dq = 0.7$ eV, and the HS state, $10\,Dq = 0.5$ eV. The IS level always lies somewhat higher and here plays no role at all. This means that at finite temperatures, $LaCoO_3$ is in a nonuniform state, in agreement with the different ionic radii of HS and LS ions. As the temperature increases, the fraction of the HS state increases. Therefore, the magnetic susceptibility as a function of temperature is well reproduced by calculation in the region of the first spin transition $T \sim 100$ K.

Despite this demonstration of the successful fitting of parameters for the CoO_6 cluster in the scenario of an LS–HS transition for the description of a number of experiments in [36], this scenario can hardly be considered final. First, there is no attempt to discuss the second spin transition at $T \sim 500$ K. Second, certain theoretical contradictions arise. Actually, the covalent admixture should be small already because of the problem setting, where the starting point is the limit of an unperturbed ionic state. This means that the weight of the d^6 configuration must dominate, while the contributions of $d^7\underline{L}$ and even more so $d^8\underline{L}^2$ must be small. Although the contributions of these configurations are not given in [36], we can still find them in similar calculations for $SrCoO_3$ [53] and $Ca_3Co_2O_6$ [73]. In [53], the weight of the ionic level d^5 for Co^{4+} in the CoO_6 octahedron is 5%, that of $d^6\underline{L}$ is 67%, and that of $d^7\underline{L}^2$ is 25%. In [73], the mean number of d electrons of Co^{3+} in cobalt in the octahedron CoO_6 is $n_d = 6.8$, that is, the covalent admixture to the ionic configuration d^6 is 80%. The large covalent admixture in the calculations in [36] manifests itself in the value of the crystal field $10\,Dq = 0.5$ eV for the HS level (and 0.7 eV for the LS level). This occurs because covalence contributes to the total crystal field, $\Delta_{tot} = 10\,Dq + \Delta_{cov}$. The d^6 configuration is required in the ionic model of the ion state for the description of EPR spectra of $LaCoO_3$ and $\Delta \approx 2$ eV (by the way, a value close to this was obtained in LDA calculations of $LaCoO_3$ and $HoCoO_3$ for the splitting of centroids of the t_{2g} and e_g bands [74]); the crystal field obtained in the calculations in [36] was $10\,Dq \approx 0.5$ eV. This means that the covalent contribution to the crystal field is far from small; in fact, it is almost three times as large as the ionic contribution. With the covalent admixture so large, the chemical bond is transformed from ionic to covalent or even to a mixture of covalent and metallic bonds. Why is it then that the crystal does not become metallic at 80% of holes on oxygen? These arguments do not allow regarding the results in [36] as putting an end to the debate concerning the nature of spin transitions in $LaCoO_3$.

The two-stage model was supported by calculations of the energies of the LS, IS, and HS levels by the method of exact diagonalization of the multiband Hamiltonian of the generalized Hubbard model for the CoO_6 cluster [75]. At low temperatures, LS becomes the ground state, and as the temperature increases, two crossovers, LS–IS and IS–HS, occur at certain parameters of the model. All three configurations are thermally populated at finite temperatures. The authors of [76] arrive at the same conclusions on the basis of electron structure calculations using the LDA method in the framework of the dynamic mean field theory (DMFT) (LDA + DMFT). In contrast to LDA + U and GGA + U calculations, this method does not require the presence of a long-range magnetic ordering and is more adequate for calculations in strongly correlated systems. The following breakdown was obtained in [76]: 45% for LS, 30% for IS, and 25% for HS.

Summarizing the discussion of the electron states and spin transitions in $LaCoO_3$, we have to recognize the absence of consensus in both theoretical and experimental studies. This means that more research is needed. In our opinion, more attention should be paid to the strong correlation of the anomalies of magnetic properties and thermal expansion.

To conclude this section, we add a few words about the possible orbital ordering in $LaCoO_3$ and other rare-earth cobaltites. As mentioned above, the presence of Jahn–Teller distortions of the crystal lattice was interpreted by a number of authors as an argument in favor of the reality of the IS state, by analogy to what happens in $LaMnO_3$, where the orbital ordering of the e_g orbitals arises owing to their half filling [60, 77]. Indeed, the IS state with a filled $d_{x^2-y^2}$ orbital is, as pointed out in [36], considerably lower in energy than with the filled d_{z^2} orbital; the reason for this is the strong orbital-dependent Coulomb interaction. All this underlies the orbital ordering shown in Fig. 5. However, this state does not have any considerable orbital moment, which contradicts the XMCD data.The nature of Jahn–Teller distortions observed in $LaCoO_3$ is based, according to [67], on the orbital triplet splitting in the crystal field with trigonal distortions. Furthermore, this splitting is precisely an illustration of the Jahn–Teller theorem, which states that the lower level is always the least degenerate one. The Co^{3+} ions in the high-spin state have a nonspherical electron shell and are capable of displaying a tendency to orbital ordering; however, the characteristics of this ordering may differ from those suggested in [43]. Indeed, as was shown in Refs [77, 78], the Jahn–Teller distortions in cobalt oxides are largely of a dynamic type, which appears to be a consequence of the instability of the magnetic state of Co^{3+} ions. In this sense, the situation in cobaltites is intermediate between those in manganites and cuprates. In manganites, the static Jahn–Teller distortions are frozen and hence inactive. In cuprates, stripe structures are observed when static distortions are realized [1], while in the case of the dynamic effect, it is averaged out as in the superconducting phase.

2.3 Magnetism, magnetoresistance, and insulator–metal transitions in the hole-doped $Ln_{1-x}M_xCoO_3$ (M = Ca, Sr, Ba) system

A considerable number of cobaltites with partially substituted rare-earth elements have been synthesized by now. Currently, nonsubstituted compositions exist as high-quality single crystals, while systems with substitutions are mostly synthesized into polycrystalline form. This is not an obstacle for their practical application, however. Quite the contrary: application-oriented experiments show that, indeed, substituted systems have higher efficiency and are therefore more promising for practical work.

Cobaltites with substituted rare-earth elements are special in a large diversity of compositions and physical properties. These compounds can be classified into two large

groups. The substituting element in the first of these groups is an isovalent rare-earth element with a different ionic radius [21, 29, 79]. In the second group, the substitution is inovalent, typically by bivalent ions of alkaline-earth elements (Ba, Ca, Sr). Among these last compounds, the best investigated are $La_{1-x}Sr_xCoO_3$ [77, 80–84].

The introduction of an element with a different ionic radius results in creating a chemical pressure that acts equivalently to external pressure. Therefore, if the ionic radius of the substituting element is smaller than that of the rare-earth ions of the original compound, then the substitution should result in additional stabilization of the low-spin state; this is indeed observed experimentally [29, 79].

The picture is much more complicated in the case of alkaline-earth substitution. Compounds realized in this case demonstrate cascades of magnetic transitions [85], colossal magnetoresistance [86], high-temperature ferromagnetism [87], charge ordering [88], electron separation of phases [77, 83], and memory effects [89]. Among the new effects are the formation of giant polarons in $La_{1-x}Sr_xCoO_3$ at very low concentrations of the alkaline-earth element ($x \sim 0.002$) [84].

One of the exceptional properties of rare-earth cobaltites with bivalent substitution is their tendency to ferromagnetic ordering: the higher the concentration of the alkaline-earth element, the greater the ordering. In addition, the ferromagnetic phase is also conducting. For example, the phase diagram of $La_{1-x}Sr_xCoO_3$ at low temperatures includes the spin-glass ($x < 0.18$) and ferromagnetic metal ($x > 0.5$) states, as well as the cluster spin-glass state [90]. A similar transition to the ferromagnetic metal state is also observed in manganites when a rare-earth element is substituted, but then it is accompanied with a structural transition that is not found in cobaltites.

The alkali-earth substitution results in the formation of Co^{4+} ions. The ground state of both the Co^{4+} ion in the highest valence state and Cu^{3+}, Ni^{3+}, and Fe^{4+} ions that are similar to it and that have the highest valence are characterized by low or even negative energy of charge transfer [91, 92]. In this case, the p–d hybridization can change the order of multiplets. A good example is found in the HTSC cuprates where the HS level $^3B_{1g}$ in the d^8 configuration has a lower energy than the LS level $^1A_{1g}$, while the levels in the $d^9\underline{L}$ configuration follow in the reverse order and the Zhang–Rice singlet $^1A_{1g}$ has the lowest energy.

In the case of Co^{4+}, the spin of the lowest HS level in the d^5 configuration is $S = 5/2$, that of the IS level is $S = 3/2$, and that of the LS level is $S = 1/2$. The mechanism of stabilization of the IS state as a result of the p–d hybridization is as follows [53]: the oxygen orbitals that hybridize with the e_g electrons of the d ion lie at a higher energy than those that hybridize with t_{2g} electrons, by the amount $2(t_{pp\sigma} - t_{pp\pi})$, where $t_{pp\sigma}$ and $t_{pp\pi}$ are the oxygen–oxygen hopping integrals for the $p\sigma$ and $p\pi$ orbitals. As a result, an oxygen hole with the e_g symmetry has a lower energy than a hole with the t_{2g} symmetry, by approximately 1.5–2.0 eV [93]. Furthermore, the hybridization parameter $t_{pp\sigma}$ is approximately twice as large as $t_{pp\pi}$. These two factors together result in stabilizing the ID level [53].

Because the LS ground state in undoped $LaCoO_3$ has almost the same energy as the HS (in the LS–HS scenario) or as both the IS and HS levels (in the two-stage model), it follows that the local lattice expansion produced by the substitution by the larger Sr^{2+} ion for the smaller La^{3+} ion reduces the crystal field and stabilizes the paramagnetic state in any of the scenarios. The emergence of magnetic centers is detected by the method of neutron scattering already at the strontium doping concentration $x = 0.002$ [84]. The behavior of the electric conductivity and thermal emf in $LnCoO_3$ cobaltites doped by electrons and holes was successfully interpreted in [94] based on the concepts of thermally stable polarons composed of high-spin Co ions in the IS state and moving in a weakly conducting LS- or LS–HS matrix.

Studies of nuclear magnetic resonance [95] and neutron scattering [77] also point to the coexistence in $La_{1-x}Sr_xCoO_3$ of ferromagnetic and nonferromagnetic nanoregions due to the tendency to phase separation. This phenomenon is well known in magnetic semiconductors [96]. Microregions enriched in holes (ferrons) have higher conductivity, in addition to the tendency to form a ferromagnetic order. An increase in the size of ferromagnetic clusters at higher substitution concentrations, or an increase caused by the magnetic field when the percolation threshold is reached, manifests itself as an insulator-to-metal transition. This mechanism causes the extraordinarily high magnetoresistance of the magnetic semiconductor EuO and seems to play an important role in the rare-earth cobaltites discussed here.

Experiments conducted in [76] showed, along with ferromagnetic correlations, that weaker antiferromagnetic correlations emerge in $La_{1-x}Sr_xCoO_3$. Because of the antiferromagnetic component in exchange interactions, antiferromagnetic ordering sets in at low temperatures [97]. Consequently, rare-earth cobaltites with alkaline-earth substitution give an impressive example of systems with competing exchange interactions of opposite signs.

The effects of charge ordering are typically observed in perovskite-structured oxides of transition metals in the cases where the relative concentration of the bivalent substitution element (and hence the concentration of the injected holes) takes integer values. This phenomenon is well known in cuprates and manganites, e.g., in $La_{15/8}Ba_{1/8}CuO_4$ [98], and in $La_{1/2}Sr_{3/2}MnO_4$ [99]. No prerequisites to charge ordering exist in stoichiometric $LnCoO_3$ compounds because all cobalt ions have the same valence and occupy the same crystallographic positions. However, there is a tendency in substituted $Ln_{1-x}M_xCoO_{3-\delta}$ systems to ordering not only different-valence cations but also oxygen vacancies. For instance, short-range ordering in the arrangement of oxygen vacancies was detected in the nonstoichiometric compound $Ho_{0.1}Sr_{0.9}CoO_{3-\delta}$ [100].

On the whole, we can conclude that the alkaline-earth substitution in perovskite-structured cobaltites leads to the formation of magnetic polarons at low concentrations, and of ferromagnetically ordered clusters and phase separation at high concentrations [101]. In a certain range of concentrations, the competition of exchange interactions of opposite signs may also stimulate the formation of spin glass. We note that the boundaries of the temperature domains of the existence of various phases depend strongly on the ionic radius of both the lantanide *Ln* and the alkaline-earth element *M*.

2.4 Ferromagnetism of nanometer-size cobaltites

As we discussed in Sections 2.1–2.3, bulk samples of $LaCoO_3$ do not typically have a long-range magnetic order. This is caused by the nonmagnetic low-spin state of Co^{3+} ions. It was all the more surprising, therefore, to discover ferromagnetic ordering in nanoparticles [102] and in epitaxial films [103] of

$LaCoO_3$. It was also discovered that both polycrystalline and single-crystal bulk specimens show the tendency to ferromagnetism in certain cases [104, 105]. The magnetic ordering temperature is in all cases approximately 85 K. A broad magnetic transition and the behavior of magnetic susceptibility are in this situation typical for cluster glasses, rather than for ordinary ferromagnets.

The interpretation of the nature of ferromagnetism in nanodimensional materials has created contradictory points of view. A hypothesis of so-called surface ferromagnetism was formulated in [106], in accordance with the fact that the spontaneous magnetic moment was found to depend strongly on the morphology of the surface and the ratio of the surface area to the volume of nanoparticles. Within the confines of this assumption, only cobalt ions on the surface of a nanoparticle (a film) are responsible for magnetic ordering. The magnetic moment of such ions is caused by distortions of their coordination.

But investigations of ferromagnetism induced in epitaxial films by tensile strength [103] showed that the magnetic moment of films increases as they become thicker; hence, a magnetically ordered state is not limited to just one surface of the film.

Another interesting interpretation of ferromagnetism in $LaCoO_3$, suggested in [107], assumes the formation of magnetic excitons in the vicinity of oxygen vacancies.

The nature of ferromagnetism in nanoparticles and $LaCoO_3$ films therefore continues to be a matter of debate. A recent study using X-ray spectroscopy [108] showed that in contrast to polycrystalline films, epitaxial $LaCoO_3$ films do not switch to the nonmagnetic state at low temperatures, which points to the 'frozen' spin state of the cobalt ions in them. In turn, the authors of Ref. [109] concluded, based on a structural and magnetic study of nanoparticles of various sizes under pressure, that the reason consists in the change of the spin state of Co^{3+} ions. This work showed that the volume of the unit cell and the length of Co–O bonds increase substantially if the particles are very small. The corresponding decrease in the crystal field induces a spin on Co^{3+} ions, while the ferromagnetic exchange results in the state of cluster spin glass. This standpoint is supported by the spectacularly pronounced suppression of ferromagnetism by hydrostatic pressure.

3. Characteristics of quasi-two-dimensional and quasi-one-dimensional cobaltites

3.1 Spin and orbital states of layered $Ln\mathrm{BaCo_2O_{5+\delta}}$ systems

Layered cobaltites — structural analogs of superconducting cuprates — can serve as examples of systems in which the mutual influence of spin, orbital, and charge degrees of freedom is most strongly pronounced. The main structural element of layered cobaltites and cuprates is the CoO_2 plane, and this permits classifying these compounds as low-dimensional systems with a great variety of phases. For example, the compound $Sr_{n+1}Co_nO_{2n+1}Cl_n$ is an insulator, whose resistance decreases with an increase in the number of CoO_2 layers n [110], and $Sr_2Y_{0.8}Ca_{0.2}Co_2O_6$ [111] is an antiferromagnetic insulator, while $Sr_2Y_{0.5}Ca_{0.5}Co_2O_7$ is a semiconductor with spin-glass magnetic ordering and clearly pronounced ferromagnetic correlations [112]. Of special interest are compounds with the K_2NiF_4 structure. Cuprates, manganites, and nickelates with this structure demonstrate spin and charge ordering as stripe structures, while ruthenates manifest exotic superconductivity [10]. The cobalt-oxide compound Sr_2CoO_4 is a ferromagnet with a relatively high Curie point [113].

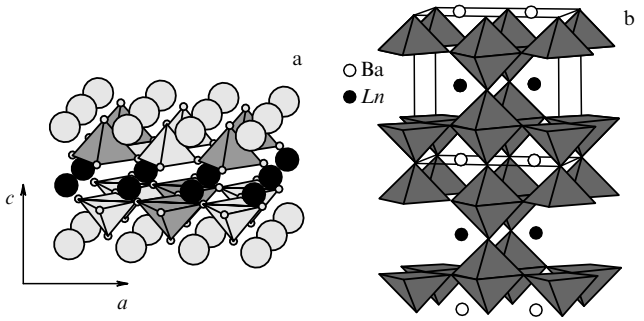

Figure 10. Crystal structure of layered cobaltites: (a) $Ln\mathrm{BaCo_2O_5}$ [115] and (b) $Ln\mathrm{BaCo_2O_{5.5}}$ [116].

Owing to their rich phase diagram, layered cobalt-oxide compounds with the general formula $Ln\mathrm{BaCo_2O_{5+\delta}}$ [114] have created a surge of interest. A spectacular feature of stoichiometric compounds of the $Ln\mathrm{BaCo_2O_{5+\delta}}$ series is that they, like superconducting cuprates based on La_2CuO_4, have dielectric properties, but cuprates may change to a superconducting behavior when doped, while doped cobaltites may display an MIT and giant magnetoresistance. We note that the transport properties are closely tied to magnetic ordering. The compounds $Ln\mathrm{BaCo_2O_{5+\delta}}$ are also made attractive by the fact that the concentration and sign of the charge carriers are easily controlled by changing the oxygen concentration. If $\delta = 0.5$, all cobalt ions are in the Co^{3+} state. By varying the oxygen concentration, the CoO_2 planes can be doped with either electrons (Co^{2+} states) or holes (Co^{4+} states). In addition to controlling the degree of band filling with charge carriers, it is also possible to vary its width by using rare-earth elements with different ion radii.

The layered cobaltites $Ln\mathrm{BaCo_2O_{5+\delta}}$ are therefore model compounds for studying the mutual effects of spin–orbit degeneration and also the kinetic and thermoelectric properties of strongly correlated electron systems.

The crystal structure of layered cobaltites is the same type as in $YBa_2Cu_3O_7$ cuprates: a sequence of layers, $[CoO_2]-[BaO]-[CoO_2]-[LnO_\delta]$ along the (001) axis. When the concentration of oxygen vacancies in the $[LnO_\delta]$ layers reaches a maximum ($\delta = 0$), each cobalt ion is inside a pyramid with a square base, formed of five oxygen ions (Fig. 10a) [115]. This forms a mixed-valence state with the $Co^{2+}:Co^{3+}$ ratio 1:1. If $\delta > 0$, then part of the cobalt ions are in an octahedral, not pyramidal, environment; at $\delta = 0.5$, the rows of pyramids and octahedra alternate (Fig. 10b) [116]. At the maximum value $\delta = 1$, Co^{3+} and Co^{4+} ions are present in equal amounts. Of maximum interest for studying the charge and orbital ordering is a comparison of two situations: (1) $\delta = 0$, with the mixed valence state realized, although the surrounding of each cobalt ion has a fivefold coordination; (2) $\delta = 0.5$, with all cobalt ions having an identical valence equal to three, but with different crystallographic surroundings.

Oxygen octahedra in layered cobaltites are strongly distorted, in contrast to octahedra in $LaCoO_3$. The same can be said about oxygen pyramids. Consequently, the aspect of the spin state of cobalt ions is even more complicated in this

situation. The crystal field produced by a pyramidal complex should be weak, and therefore a transition metal ion in a pyramidal environment should manifest the tendency to a nonzero spin state. The evolution of the spin state of a transition metal ion in the pyramidal environment was analyzed in detail in [117], and it was shown that both the HS state and the IS state can be the ground state depending on the nature and degree of distortion of the ligand complex. A calculation of the electron levels of a Co^{3+} ion in pyramidal surroundings in [118] yielded only the HS state as a candidate for the possible ground state, while the authors of theoretical paper [119] concluded that only the IS state can be stable. No consistent calculation of the electron structure of cobalt ions taking the spin–orbit interaction, covalence, and strong electron correlations into account has been carried out so far; relevant conclusions drawn in experimental papers continue to disagree.

Charge ordering is a typical phenomenon in the family of layered cobaltites. Charge ordering is observed even in materials having a single type of crystallographic position for a transition metal ion. For instance, in layered $LnBaCo_2O_5$ (Ln = Tb, Dy, Ho) perovskites, two structural transitions were found: at $T_N \approx 340$ K and $T_{CO} \approx 210$ K [120, 121]. The first of these structural transitions is connected with the establishment of a long-range antiferromagnetic order, and the second, with charge ordering. The presence of charge ordering was established directly by observing an additional superstructural peak in the neutron and electron diffraction spectra. Indirect evidence of the implementation of this phenomenon was also found in the data of differential thermal analysis and conductivity. In the $LnBaCo_2O_5$ compounds, charge ordering results in doubling the unit cell; this implies that pyramidal complexes surrounding Co^{3+} ions are smaller in size than in the case of Co^{2+}. The magnetic moment of different-valence ions changes from ion to ion, and the difference between saturation magnetizations corresponding to different states equals $1\mu_B$.

A much richer palette of phenomena can be observed in $LnBaCo_2O_{5+\delta}$ compounds, which demonstrate a plethora of phases depending on the sort of the rare-earth element and the concentration δ of oxygen vacancies. Of special interest among the phenomena observed in these materials are the unusual magnetic transition between the antiferromagnetic (AFM) and ferromagnetic (FM) states at $T_M \approx 220-270$ K, the metal–insulator transition at $T_{MI} \approx 310-360$ K, giant magnetoresistance in the vicinity of T_M, and anomalous distortion of the crystal lattice in the vicinity of T_{MI} [122–126]. The magnetic ground state of these materials is a state with the AFM ordering, which indeed sets in at low temperatures. But as the temperature increases, ferromagnetism arises in the system, although it exists only in a relatively narrow temperature range.

The corresponding temperature dependence of magnetization is very unusual and has a peak close to T_M (Fig. 11) [127–129]. It was also discovered in [86, 129] that the magnetic behavior of high-quality single crystals of $GdBaCo_2O_{5.5}$ has a strongly pronounced anisotropic Ising character; the magnetic field stimulates the AFM state to switch to the FM state, which is accompanied by giant magnetoresistance arising in the specimen. The interpretation suggested by the authors of these papers using the totality of experimental data is based on the spin and orbital ordering of Co^{3+} ions. The authors of [129] are of the opinion that the structure arising in $GdBaCo_2O_{5.5}$ is formed of planes with Co^{3+} ions in various

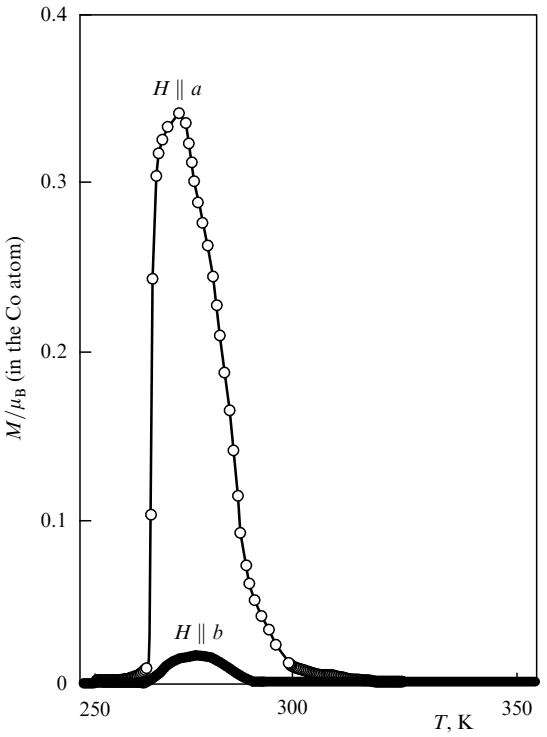

Figure 11. Anisotropic magnetization of $GdBaCoO_{5.5}$ as a function of temperature [86].

spin states. The positions of the cobalt ions are not equivalent because oxygen ions are ordered into alternating empty and filled chains. Incidentally, octahedrally surrounded Co^{3+} ions are nonmagnetic, while pyramidally surrounded ions have a magnetic moment (Fig. 12). The authors of Ref. [129] assume that Co^{3+} ions in a pyramidal environment are in the IS state. Their magnetic moments are then oriented along oxygen chains. The plane-to-plane interaction at low temperatures across Co^{3+} ions in the LS state is weak and has an antiferromagnetic nature. As the temperature increases, some Co^{3+} ions among previously nonmagnetic planes acquire a magnetic moment, after which an additional indirect exchange interaction orders the planes ferromagnetically. The mechanism of giant magnetoresistance then consists in a reorientation of magnetically ordered layers weakly bound to one another; this in turn affects charge transport. Layered $Ln_{0.5}Ba_{0.5}Co_2O_{5.5}$ cobaltites are narrow-gap insulators in which charge carriers are produced by forming $Co^{3+}-Co^{4+}$ pairs. The energy of these excitations depends on the magnetic order. Indeed, each thermally excited state in a low-spin Co–O layer is strongly bound to two neighboring magnetically ordered layers, joining them through a ferromagnetic 'bridge.' The relative magnetic ordering of layers can appreciably change the width of the dielectric gap. An applied magnetic field ferromagnetically orders the layers and reduces the gap width, which sharply increases the number of charge carriers and enhances conductivity.

Experiments with neutron scattering combined with group-theory analysis in [128] for $YBaCo_2O_{5+\delta}$ showed that the real situation may be more complex than assumed by authors of earlier papers [86, 129]. It was thus established that nonequivalent positions exist even within the octahedral and pyramidal sublattices. The formation of superstructures also brings about a more complicated scenario of magnetic

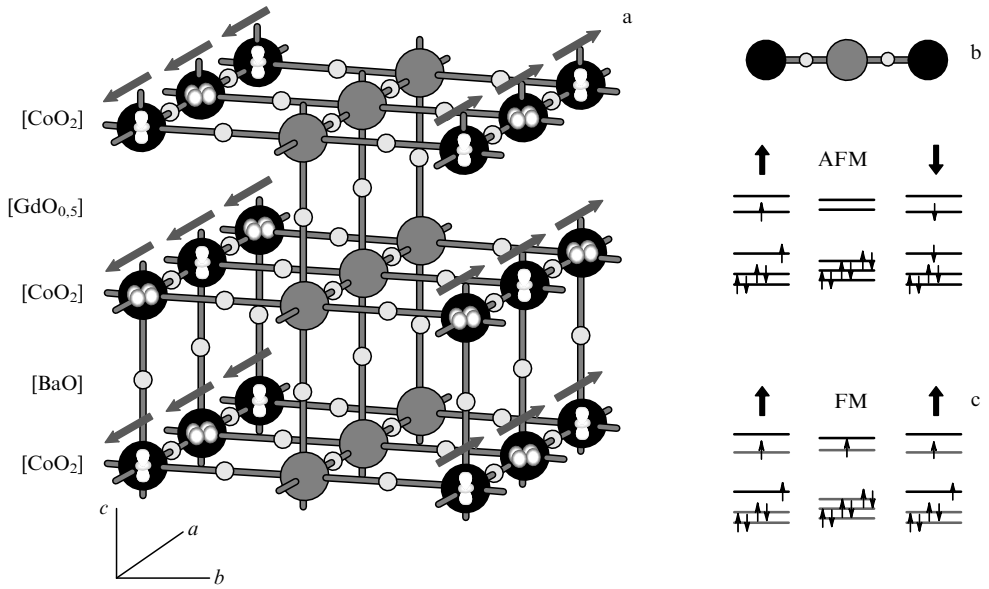

Figure 12. Crystal and magnetic structures of $GdBaCo_2O_{5.5}$. (a, b) AFM ordering in the case of Co^{3+} ions alternating in the IS and LS states, (c) switching into an FM state in the presence of Co^{2+} ions [86].

ordering. In the opinion of the authors of [128], a spontaneous magnetic moment arises in the octahedral sublattice with a staggered alternation of Co^{3+} ions in the LS and IS states. The driving force of the magnetic phase transition is the thermal excitation of the magnetic moment in diamagnetic Co ions. At low temperatures, these excitations produce magnetic frustrations that presumably provoke the formation of two different types of antiferromagnetic ordering and spin-based phase separation [130].

Layered cobaltites allow observation of the concentrational metal–insulator transition owing to the possibility of controlling the degree of doping by charge carriers with the opposite sign. An interesting and unusual mechanism of spin blockade that describes the transition from hopping to band conductivity in rare-earth cobaltites was suggested in [131]. We know that the concentration of oxygen vacancies critically affects the transport and thermoelectric properties of layered cobaltites. A strongly pronounced MIT is observed in compounds with $x \approx 0.5$. The low-temperature resistance has a hopping Mott nature in the wide range $0 \leqslant x \leqslant 0.7$; this allows regarding the transfer process as hopping by localized electrons (Co^{2+}) or holes (Co^{4+}). The mechanism of spin blockade shown schematically in Fig. 13 is an indication that the processes of transfer for electrons and holes in a matrix of cobalt ions in different spin states operate differently. Almost localized t_{2g} holes can move along the matrix consisting of cobalt ions in the LS state (Fig. 13a), but the conductivity is hopping in nature, as we observe at low temperatures. Moreover, electron hopping is forbidden (Fig. 13b) because it forces a change in the spin state of cobalt ions with an exchange of an electron from a low-spin to a 'wrong' high-spin state. At higher temperatures, when most cobalt ions transfer to the nonzero-spin state, the electron transfer is 'allowed' (Fig. 13c). The corresponding band is then wider and the conductivity ceases to be hopping in nature. The stark asymmetry of conductivity when the compounds $GdBaCo_2O_{5+\delta}$ and $NdBaCo_2O_{5+\delta}$ [16, 132] are doped with electrons and holes supports this hypothesis.

A characteristic feature of cobaltites that makes them stand out from the families of other oxides of transition

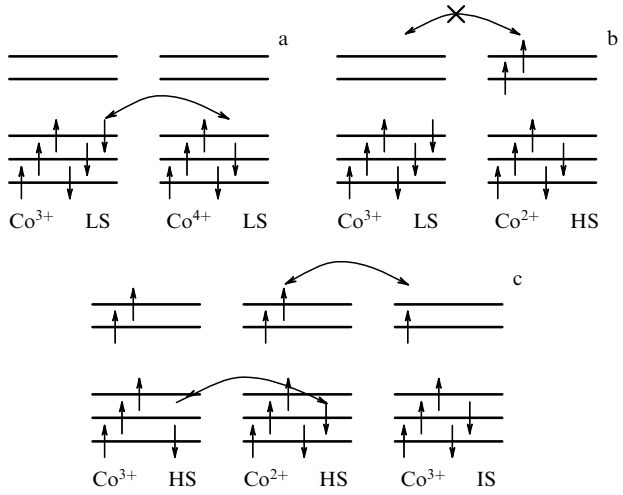

Figure 13. Diagram of the process of hole hopping (a) and electron hopping (b) on a matrix of Co^{3+} ions in different spin states (the 'spin blockade' conductivity mechanism) [131].

metals is the high thermal emf. For instance, even though layered $Na_xCoO_2 \cdot yH_2O$ cobaltites attract attention owing to their superconducting properties, the basis compound Na_xCoO_2 is known precisely due to its thermoelectric properties [133]. It was discovered that Na_xCoO_2 at $x = 0.6$ simultaneously has the metallic conductivity, a low thermal conductivity, and a high thermal emf. A combination of these properties allows treating Na_xCoO_2 as an efficient material for thermoelectric cooling. $La_{1-x}Sr_xCoO_3$ also has a high thermal emf [80, 90]. The anomalous behavior of the Seebeck coefficient for $GdBaCo_2O_{5+\delta}$ and $NdBaCo_2O_{5+\delta}$ manifests itself in its different and nonmonotonic temperature dependence at different concentrations (Fig. 14) [16]. In cobaltites, the thermal emf undergoes sharp changes in the region around the metal–insulator transition. In the highly conducting phase, the thermal emf is low and negative, which points to the electron nature of charge transfer. In the insulating region, the thermal emf

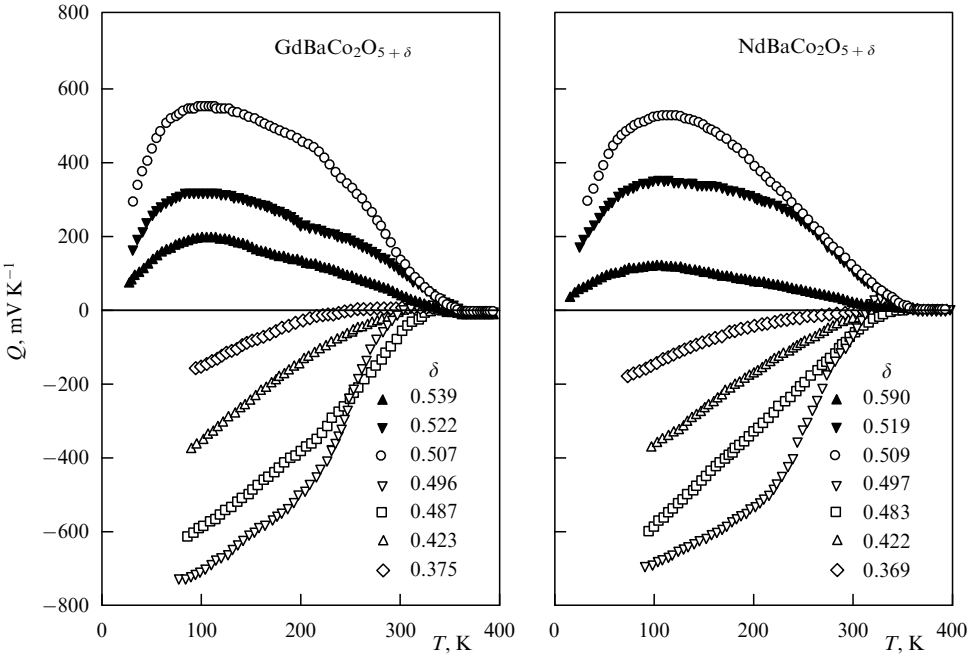

Figure 14. The Seebeck coefficient of $GdBaCo_2O_{5+\delta}$ and $NdBaCo_2O_{5+\delta}$ as a function of temperature [16].

reaches a maximum at $\delta \approx 0.5$ and decreases appreciably after doping with both holes and electrons, in contrast to the asymmetric behavior of resistance. This behavior of the thermal emf is not typical of ordinary semiconductors. A thermodynamic analysis in [16] shows that the decisive factor in cobalt oxide compounds is the entropic contribution to the thermal emf. The high values of entropy are here due to the spin and orbital instability of magnetic cobalt ions, which is closely related to the lattice and charge degrees of freedom.

3.2 Correlation of orbital ordering and magnetic and electron transitions in layered $La_{1-x}Sr_{1+x}CoO_4$

There are compounds in the family of cobalt oxide materials that constitute structural analogs of superconducting cuprates. These are cobaltites with the general formula Ln_2CoO_4. This class of materials has been studied in much less detail than pseudocubic $LnCoO_3$ cobaltites.

The crystal structure type of Ln_2CoO_4 is K_2NiF_4 formed of alternating layers of $LnCoO_3$ perovskite and LnO rock salt. Cobalt ions in stoichiometric compounds of this family are bivalent and their electron configuration is d^7.

The compound La_2CoO_4 has unusual magnetic properties. At low temperatures, it is an AFM insulator ($T_N = 228$ K) [134]. At the temperature $T_2 = 103$ K, a magnetic transition occurs to a different, equally antiferromagnetic phase. Moreover, this magnetic transition is accompanied by a structural transition from the rhombic to the tetragonal phase. The behavior of magnetization in La_2CoO_4 points to a clearly pronounced anisotropy. As follows from the neutron diffraction data [134] obtained using a single crystal specimen of $La_2CoO_{4.15}$ at temperatures below 227 K, long-range magnetic ordering is observed in this compound, and at a temperature near 103 K, spins rotate in the basis plane as a transition to a new antiferromagnetic phase occurs. This magnetic transition is connected with a first-order structural phase transition, from the high-temperature orthorhombic phase to the low-temperature tetragonal phase.

Transformations occurring in La_2CoO_4 when strontium is substituted for lanthanum are very unusual. The compound $La_{2-x}Sr_xCoO_4$ demonstrates a concentrational spin transition accompanied by a complex magnetic and electronic behavior [135]. Photoemission spectra [136] and transport data [137] indicate that an MIT exists in this system in the vicinity of $x = 0.2$. Furthermore, this transition corresponds to a magnetic transition from a nonmagnetic to a ferromagnetic state. To clarify the nature of the spin transition in doped cobaltites, the electron structure of perovskite $La_{1-x}Sr_xCoO_3$ was calculated in [138] in the range of concentrations $0 < x < 1$; the calculation showed that the ground state of cobalt ions changes from LS ($t_{2g}^{6-x}e_g^0$) at low doping concentrations $x < 0.25$ to IS ($t_{2g}^5e_g^{1-x}$) at $0.25 \leqslant x \leqslant 0.41$. As x increases from $x = 0.41$, cobalt ions change to a HS state ($t_{2g}^4e_g^{2-x}$) and are shown to be all in this state at $x = 1$. For $x \geqslant 0.25$, the spins are ferromagnetically ordered.

Such unusual magnetic properties are not a unique feature of the isotropic perovskite $La_{1-x}Sr_xCoO_3$; they are also observed in the layered compound $La_{2-x}Sr_xCoO_4$. The results of studies of nuclear magnetic resonance (NMR) in a zero field [139] showed that the magnetic state of this material changes stepwise from an AFM to an FM state for $x \geqslant 0.6$. The effective magnetic moment decreases slowly beginning from $x \sim 0.5$ [140], which is followed by a sharp drop at $x \sim 0.7$. The process is accompanied by a considerable decrease in the electric resistance. These experimental data allowed the authors of [140] to advance the hypothesis that Co^{3+} ions go through a transition from the HS to the IS state at $x \sim 0.7$. However, as follows from the neutron diffraction data [141], the cobalt ions in $LaSrCoO_4$ are in the LS and HS states in a 1:1 ratio at low temperatures. This is also confirmed by the optical conduction spectra [142].

The Hartree–Fock calculation of the band structure of $La_{2-x}Sr_xCoO_4$ in [143] in the wide range of concentrations

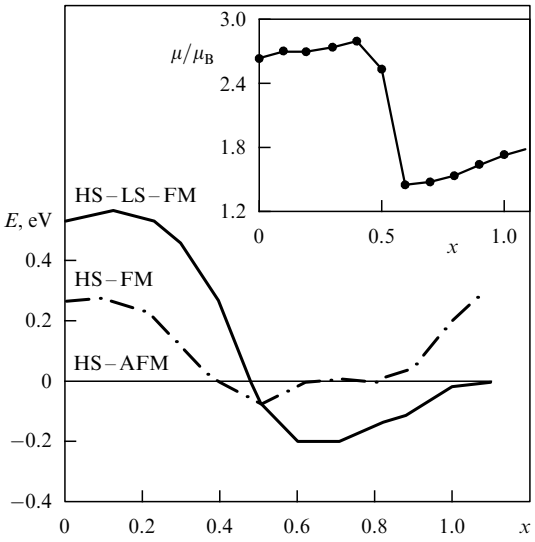

Figure 15. Relative energies of spin states of cobalt ions in $La_{2-x}Sr_xCoO_4$ as a function of concentration [143]. The inset shows the experimental curve of the magnetic moment per double unit cell.

$0 < x < 1.1$ reproduced the experimental dependence of the magnetic moment. The results of the theoretical calculation yielded the AFM-ordered HS state $(t_{2g}^{5-x}e_g^2)$ for $0 < x < 0.39$ and the ferromagnetic HS state $(t_{2g}^5e_g^{2-x})$ for $0.39 \leqslant x < 0.52$. For $0.52 \leqslant x < 1.1$, the ferromagnetic HS–LS-ordered state is realized. Therefore, two spin transitions occur in the above range of concentrations. The relative energies of the states obtained are plotted in Fig. 15 [143], where a cascade of spin crossovers is well pronounced in the concentration range 0.39–0.52. Band calculations [143] show the presence of a strong O-2p–Co-3d hybridization; in addition to magnetic properties, these calculations qualitatively yield the MIT that occurs when the Fermi level crosses the top of the valence band. According to [143], this occurs in the concentration range $x \sim 0.3$.

3.3 Charge, spin, and orbital states of Co ions in quasi-one-dimensional $Ca_3Co_2O_8$ crystals

It follows from the results in Section 3.2 that lowering the structural dimensionality in cobalt oxides produces a number of new magnetic and electronic properties due to the peculiarities of spin, charge, and orbital ordering. Another representative of low-dimension cobalt oxides is the quasi-one-dimensional cobaltite $Ca_3Co_2O_6$.

The rhombohedral crystal structure of this compound is formed of CoO_6 chains stretched along the corresponding hexagonal unit cell axis. Each chain is a sequence of alternating CoO_6 octahedra and trigonal CoO_6 prisms (Fig. 16) [144]. According to the neutron diffraction data, the ferromagnetic exchange interaction is predominant inside the chains (in the direction of the c axis), while the antiferromagnetic interaction dominates between chains (in the ab plane) [145]. The magnetic moment of a chain is $4.8\mu_B$, and the spin freezing temperature is $T = 7$ K. The aniferromagnetic ordering temperature is $T_N = 25$ K [146]. At low temperatures, this compound undergoes a transition induced by a magnetic field from the ferrimagnetic to the ferromagnetic state [146, 147].

The separation between cobalt ions inside a chain is 2.9 Å, which is much less than the separation between chains (equal

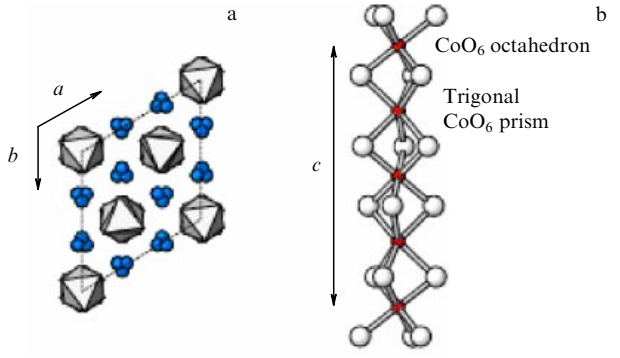

Figure 16. (a) Projection of the structure of $Ca_3Co_2O_6$ onto the (001) plane shows a triangular ordering of chains. (b) Chains of cobalt ions in octahedral and prismatic environments [144].

to 5.3 Å). Therefore, exchange interactions within chains are much stronger than between chains, and the magnetism in $Ca_3Co_2O_6$ can be described in terms of a triangular Ising lattice in which the magnetic moment of each chain plays the role of one spin. The antiferromagnetic exchange between chains produces frustration of magnetic ordering, which manifests itself in an extremely unusual stepwise behavior of magnetization curves in these compounds. Typical curves are plotted in Fig. 17a [144]. As follows from Fig. 17a, the magnetization curve contains a number of steps. The authors of [144] relate them to the presence of various magnetic superstructures, which are schematically shown in Fig. 17b. Provisionally setting the magnetic moment of one chain to unity, we see that the magnetic moment of the Co_3 triangle can be -1, $+1$, or $+3$, as shown in the inset in Fig. 17b. An applied magnetic field induces some chains to rotate and causes changes in the two-dimensionally ordered array of triangles. The ratio of magnetizations of these superstructures corresponds to the height of the steps on the $M(H)$ curve at $T = 2$ K. Despite the very good qualitative agreement of the magnetization curve with the model suggested, the unusual magnetic properties of $Ca_3Co_2O_6$ can also be explained using alternative models. As remarked in [148], similar steps on magnetization curves develop in structures with magnetic clusters (Mn_{12}, Fe_8, etc.); the steps correspond to the tunneling of microspins related to these clusters [149].

Modern neutron diffraction data demonstrate that the magnetic structure of $Ca_3Co_2O_6$ is significantly more complex than that corresponding to ferrimagnetic ordering in a triangular lattice. The magnetic structure of $Ca_3Co_2O_6$ is a longitudinal (along the c axis) sine-modulated structure with a very large period [150]. The authors of Ref. [150] insist on the need to take the three-dimensional helicoidal nature of interactions and a combination of short- and long-range magnetic orders into account.

The problem of the spin state of cobalt ions is very acute for $Ca_3Co_2O_6$, just as it is for other cobaltites. It is claimed on the basis of the results of density functional calculations in [151] that the octahedral Co_{oct} positions are occupied by Co^{4+} ions in the LS state, while the trigonal Co_{trig} positions are occupied by HS ions Co^{2+}. According to other experimental and theoretical publications, however, all cobalt ions are trivalent and Co_{oct} are in the LS state and Co_{trig} are in the HS state [152–154].

There is no clear understanding of the nature of Ising magnetism in $Ca_3Co_2O_6$ either. In [155, 156], this phenom-

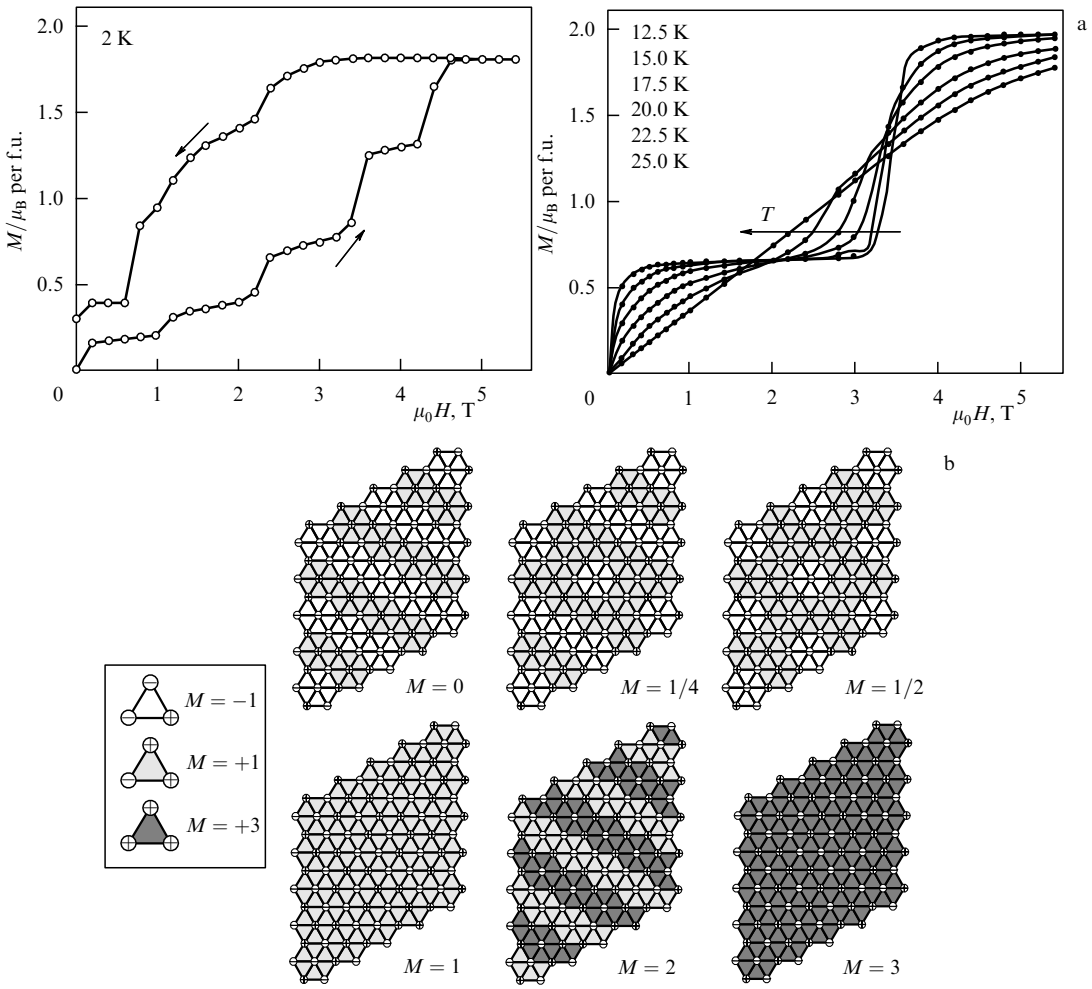

Figure 17. (a) Magnetization curves of $Ca_3Co_2O_6$ (μ_0 is the magnetic constant and H is the magnetic field strength). (b) Models of the magnetic structures of $Ca_3Co_2O_6$ [144].

enon is discussed from two different standpoints. According to [155], the ground level for the cobalt ion in a prismatic environment is the magnetically inactive orbital state d_0, but according to [156], the active d_2 orbital lies at a somewhat lower energy. In [156], it was concluded from experiments on X-ray spectroscopy and magnetic circular dichroism that the valence of all cobalt ions in $Ca_3Co_2O_6$ is equal to +3 and that the ion spin state agrees with the results in [152–154]. An anomalously large orbital moment 1.7 μ_B was found in Co_{trig}, which the authors of [73] relate to the double occupancy of the d_2 orbital. A detailed analysis of spectral lines while jointly taking the magnetocrystalline anisotropy into account points to the impossibility of the existence of an orbitally inactive d_0 level and the ground state. This, in turn, means that the spin–orbit interaction must be taken into account in calculations of the band structure of $Ca_3Co_2O_6$.

4. Layered $Na_xCoO_2 \cdot yH_2O$ cobaltites with a triangular lattice

4.1 Crystal structure and phase diagram

As noted above, the interest in layered Na_xCoO_2 cobaltites arose in view of the high values of thermal emf [133]. But these cobaltites became a truly 'hot' subject of research only several years later, after unusual superconductivity had been discovered in $Na_xCoO_2 \cdot yH_2O$ [12]. One of the reasons for the growing interest in layered cobaltites based on Na_xCoO_2 is that systematic theoretical and experimental studies of this novel superconducting system may help in comparing the mechanisms of superconductivity in cobaltites and traditional cuprate-based HTSC materials. The crystal structure of the base compound Na_xCoO_2 is quasi-two-dimensional in nature and consists of electrically active CoO_2 planes. These planes are separated by Na layers that act like charge reservoirs (Fig. 18) [12, 157]. Cobalt ions form a triangular lattice. For example, $Na_{0.61}CoO_2$ crystallizes at $T \approx 12$ K into a hexagonal structure (the group $P6_3/mmc$) with the lattice parameters $a = 2.83176$ Å and $c = 10.84312$ Å [158]. Oxygen sits in a high-symmetry 2d $(1/3, 2/3, 3/4)$ position, and the Co–O distance is 1.9072(4) Å. After intercalation of water, H_2O molecules settle in the neighborhood of sodium ions and lead to an increase in the lattice parameter c, that is, an effective increase in quasi-two-dimensionality.

As in the case of cuprates, the phase diagram of $Na_xCoO_2 \cdot yH_2O$ includes several competing electron phases and displays complexity and diversity (Fig. 19). Both the deficit of sodium ions x and the degree of hydration y affect the physical properties. In addition to the superconducting state, which appears in response to the intercalation of water, the phase diagram shows the presence of magnetically ordered and charge-ordered states, as well as several structurally different phases.

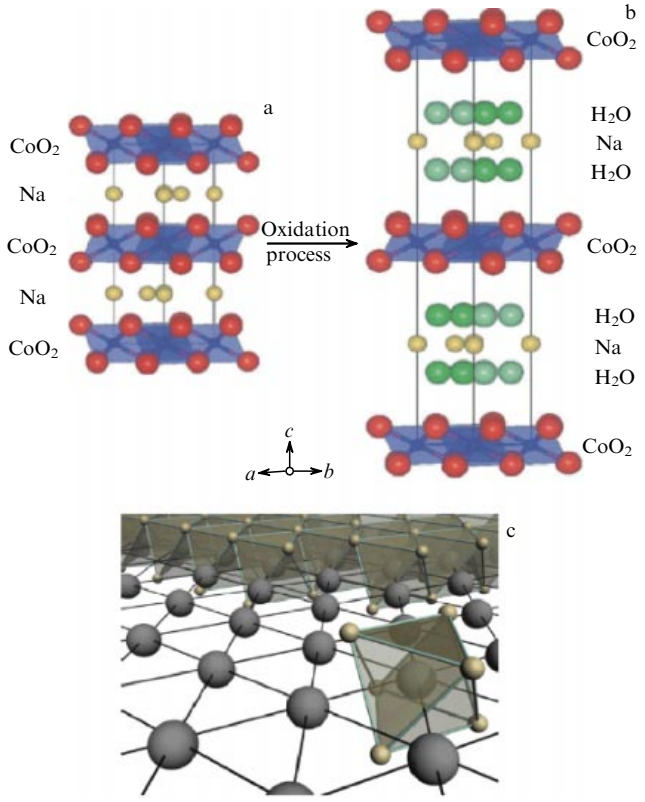

Figure 18. (a) Crystal structure of Na_xCoO_2. (b) Evolution of this structure in the process of intercalation of water [12]. (c) A CoO_2 layer in which larger spheres correspond to Co and smaller ones to O.

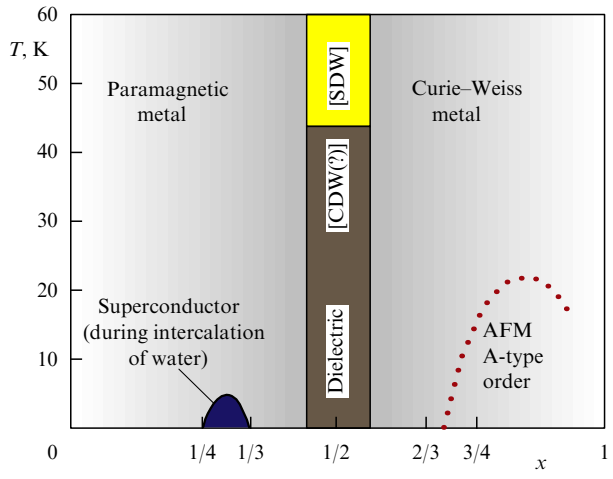

Figure 19. Phase diagram of $Na_xCoO_2 \cdot yH_2O$. (CDW: charge density wave; SDW: spin density wave.)

Judging by the electric conductivity, $Na_xCoO_2 \cdot yH_2O$ is a good metal at low temperatures in the entire range of concentrations except in the neighborhood of the point $x = 1/2$, where an insulating state is created [159]. At high temperatures $T > 300$ K, ionic conductivity arises in the layered cobaltite as a consequence of the mobility of Na ions.

One of the first systematic studies of the magnetic properties of Na_xCoO_2 as functions of concentration was conducted in [159]. At low concentrations up to $x = 1/2$, the magnetic behavior of Na_xCoO_2 has a familiar paramagnetic

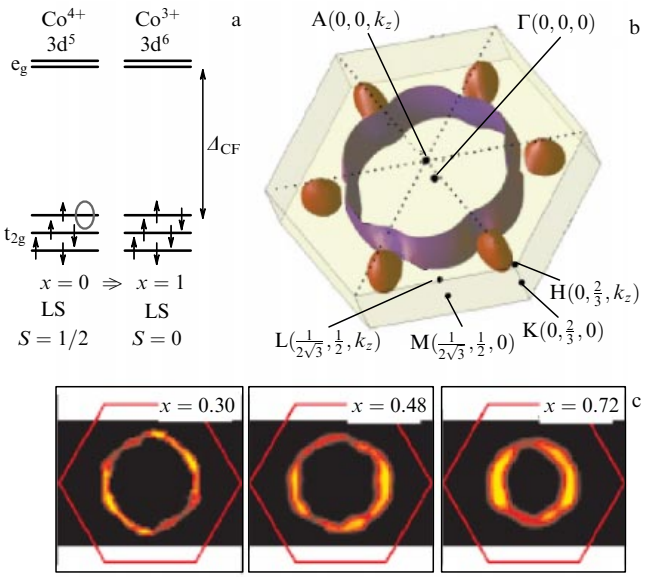

Figure 20. (a) Diagram of Co energy levels near the Fermi level in Na_xCoO_2 and their population as the doping level is increased for an LS configuration. According to band calculations, the crystal field Δ_{CF} is equal to 2 eV [210]. (b) The Fermi surface of $Na_{0.33}CoO_2$ in the hexagonal Brillouin zone obtained by an LDA calculation [184]. (c) The Fermi surface of Na_xCoO_2 for different concentrations x, measured by the ARPES technique [175].

character, but the magnetic susceptibility is twice as high as the Pauli susceptibility. The superconducting state arises in the range of concentrations $1/4 < x < 1/3$ [157, 160]. As x increases further, the susceptibility again acquires the Curie–Weiss nature, with the Curie paramagnetic point approximately equal to 70 K. A second-order transition to an ordered phase was found at $x > 2/3$ and $T \approx 22$ K [161]. Further investigation using muon and neutron scattering showed that this phase corresponds to the type-A long-range order, i.e., Co spins in the plane are ferromagnetically ordered with $J_{ab} = -6$ meV, and the exchange along the c axis is antiferromagnetic, $J_c = 12$ meV [162–165]. Curiously, an anomalously high thermo-emf is observed in the same range of concentrations [133, 166–168]; it is suppressed by the magnetic field [169]. This may point to its entropic nature connected to the hopping of strongly correlated holes.

4.2 Electron structure

In contrast to HTSC cuprates, in which the Cu^{2+} ion configuration is $3d^9$ and a hole occupies the only unoccupied e_g orbital, cobaltites are essentially multiorbital systems. The electrons given by Na ions to the CoO_2 layer decrease the valence of cobalt from Co^{4+} ($3d^5$) to Co^{3+} ($3d^6$) as x varies from 0 for CoO_2 to 1 for $NaCoO_2$, which is a band insulator. A hole in the d orbital occupies one of the t_{2g} levels located lower than the e_g levels by $\Delta_{CF} \approx 2$ eV [159] (Fig. 20a). The degeneration of the t_{2g} levels is partly removed by a trigonal crystal field, which splits them into a singlet a_{1g} and two lower e_g' levels.

The study of the electron structure of superconducting cobaltites highlighted a number of problems; the most acute of them is the discrepancy between first-principle calculations in the LDA framework and ARPES (angle-resolved photoelectron spectroscopy) data. At $x = 0.33$, LDA-based calculations yield a large Fermi surface in the neighborhood of the

Γ point of the Brillouin zone, mostly connected with a_{1g} states, and six small pockets mostly of the e_g' type in the neighborhood of K points [157, 170–172] (Fig. 20b). But according to ARPES data, only one hole Fermi surface exists around the Γ point, in a wide range of Na concentrations [173–179]. Bands to which the e_g' orbitals contribute lie at a lower level and never intersect the Fermi level.

The absence of e_g' pockets is unexpected and imposes serious limitations on a number of suggested models with nonphonon superconductivity mechanisms and also on the magnetic properties stemming from the nesting condition [171, 180, 181]. Moreover, the measured quasiparticle band width is approximately twice as small as that following from LDA calculations. This substantial contradiction between the ARPES and LDA results can be resolved in one of two ways: by including the effects of strong electron correlations into the picture and going beyond the LDA, or by reconsidering the correctness of ARPES results. We consider both options here.

The effects of local Coulomb repulsion treated by combining the LDA with the Hubbard model (the local spin density approximation, LSDA, and LSDA + U) reproduce the absence of small pockets on the Fermi surface [182]. But this results in a totally polarized ferromagnetic state, a band split in spin, and a spin-polarized Fermi surface twice as big in area. All this contradicts the experimental data. An attempt to explain how strong electron correlations produce orbital polarization and the ARPES-observed band narrowing has been made in [183, 184]. Using the model of t_{2g} bands with dispersion taken from LDA calculations, and also the Gutzwiller approximation [185–187], the authors of [183, 184] found that pockets are absent on the Fermi surface for concentrations $x > 0.2$ because the strong Coulomb repulsion shifts the e_g' band to below the Fermi level, thus creating an orbitally polarized state with a single cylindrical Fermi surface centered at the Γ point.

On the other hand, calculations based on the multiorbital Hubbard model and DMFT have established that pockets on the Fermi surface must be even larger than predicted by the LDA [189]. The contradiction between the results of the two theories for strongly correlated systems, the mean field theory (the Gutzwiller approximation) and the DMFT, were resolved in [190]. It was shown that the DMFT gives the same results as the Gutzwiller approximation if the initial splitting Δ_{ae} of the levels a_{1g} and e_g' is positive, i.e., the e_g' levels lie at a lower energy. We note that this result is independent of the magnitude of the Hubbard repulsion U and the Hund exchange J. Hence, the sign of Δ_{ae} is qualitatively important. Fine-tuning of the dispersion in the multiorbital model of strong bonding (five d orbitals of Co and three p orbitals of O) in the LDA framework gave the value $\Delta_{ae} = -200$ meV for $x = 0.3$ [171]. When LDA calculations are projected onto the tight-binding model for the Co t_{2g} orbitals, the result is $\Delta_{ae} = 53$ meV [184], while the alternative procedure for calculating the splitting parameter yielded the value −144 meV [191]. Quantum chemistry methods yielded a positive value of splitting equal to 315 meV [192]. In order to bring order to the matter of calculating the splitting parameter, a first-principle calculation of Δ_{ae} was conducted in [193] taking two CoO_2 layers per unit cell into account, without projecting onto the tight-binding model. It became clear that the result is affected by Na ions that were taken into account without using the virtual crystal or any other approximation. Eventually, the authors of [193] arrived at a negative value of Δ_{ae} of the order of −100 meV. This means that even with the effects of strong correlations taken into account, the e_g' hole pockets must survive on the Fermi surface at high concentrations up to $x \approx 2/3$, assuming, of course, that we rely on the DMFT results. In reality, this theory cannot be justified in the two-dimensional case because the inverse spatial dimension is not small. Furthermore, the mass operator in the DMFT approximation is independent of the quasimomentum, and hence any description of the fine points of the dispersion law and Fermi surface would be beyond the efficacy of these calculations. The Gutzwiller approximation used in [183, 184] is a good interpolating solution in the theory of metallic strongly correlated systems and its results are more reliable in this particular case. Therefore, it appears that the correctness of conclusions from ARPES experiments is questionable.

In contrast to ARPES data, the detection of Shubnikov–de Haas quantum oscillations points to the presence of small sections of the Fermi surface, both for systems with $x = 0.3$ and for $Na_{0.5}CoO_2$ [194, 195]. The authors of [194] found that the frequencies of quantum oscillations for $x = 0.3$ are in good agreement with the results of LDA calculations [157]. This interpretation was rejected, however, because the experimentally observed specific heat value $\gamma_n = 12$ mJ K^{-2} mol^{-1} [196, 197] is less than the quantity obtained from theoretical estimates in the case of six e_g' pockets. On the other hand, new measurements of specific heat give the value $\gamma_n = 16.1$ mJ K^{-2} mol^{-1} [198], which is not very different from theoretical estimates. Another experiment demonstrating the presence of small pockets is Compton scattering [199].

To summarize, the totality of experimental data demonstrating the presence of small e_g' pockets at $x < 2/3$ warrants doubting the ARPES results. So far, we know the only answer to the question of why ARPES fails to see small pockets. This can be explained in terms of either the extreme sensitivity of the ARPES method to details of the specimen surface [171, 191, 199, 200] or the smallness of the matrix elements of dipole transitions for the appropriate wave vectors. We thus see that neither the theory nor experiments currently provide reliable results for the Fermi surface in Na_xCoO_2.

4.3 Dielectric state in the vicinity of $x = 0.5$

The most spectacular and utterly unusual feature of the phase diagram of $Na_xCoO_2 \cdot yH_2O$ is allegedly the presence of a narrow region corresponding to a dielectric state in the vicinity of $x = 1/2$. This state corresponds to the temperature dependence of susceptibility with two peaks at $T_{SDW} = 88$ K and $T_{MI} = 53$ K [159, 201]. Electric resistance changes monotonically on passing through T_{SDW} but undergoes an abrupt jump at T_{MI}. An investigation of the electron diffraction revealed a superstructure in the arrangement of sodium ions [159, 201, 202].

The state at $T < T_{SDW}$ was initially associated with charge ordering of Co induced by the Na superstructure; Na ions at $x = 0.5$ occupy two nonequivalent positions. One of them, denoted by Na1, is located right above Co in the plane, and the other (Na2) lies at the midpoint of the triangle formed by cobalt ions. If Na in the Na1 position yielded all its electrons to cobalt, then cobalt would change its state to Co^{3+}. All other cobalt ions would be in the Co^{4+} state with the spin $S = 1/2$. This charge segregation in chains of nonmagnetic Co^{3+} ions and magnetic Co^{4+} ions would create a dielectric

magnetic state [159, 202]. However, this interpretation fails to explain why a dielectric state is formed only at temperatures lower than T_{MI}, while Na ions are observed to order at room temperature as well. Nor has an explanation been found for T_{SDW} not being equal to T_{MI}.

An alternative interpretation was suggested based on the data of NMR and neutron scattering experiments [197, 203–206]. First, these experiments showed that charge ordering does not follow the scenario outlined above. Namely, the valences of cobalt chains are $Co^{3.5+\delta}$ and $Co^{3.5-\delta}$, where $\delta < 0.1$. The temperature of this charge ordering is higher than T_{SDW} and approaches $T_{CO} \approx 150$ K [204]. Second, the valence of cobalt does not change on passing across T_{SDW} [203]. Therefore, T_{SDW} has no direct connection to charge ordering, and the available set of experimental data allows classifying the state at $T < T_{SDW}$ as a magnetic order of the spin density wave type [203].

On the other hand, this scenario leaves the situation with the transition at T_{MI} unresolved. Part of NMR data indicate no charge ordering at temperatures $T < T_{MI}$, and the authors of [203] suggest interpreting T_{MI} as the temperature of yet another transition to the state with a *spin* density wave and the reconstruction of the Fermi surface, such that it produces a small amount of charge carriers. The NMR data of another group permitted the authors of [205] to discuss the transition at T_{MI} to a *charge* density wave. Obviously, further experimental work is required to resolve the issue of the nature of the transition in $Na_{0.5}CoO_2$ at $T_{MI} = 53$ K.

4.4 Nature of superconductivity and magnetism

The behavior of magnetic susceptibility in Na_xCoO_2 does acquire features characteristic of the behavior of magnetic susceptibility in magnetically ordered substances, but only at high concentrations of Na ions ($x > 0.75$). In this concentration range, Na_xCoO_2 is a type-A antiferromagnetic metal with ferromagnetically ordered Co spins in the planes and antiferromagnetic ones between planes. According to NMR data, ferromagnetic spin fluctuations become considerable in the metallic region at concentrations $x > 0.67$ [207], while the data of nuclear quadrupole resonance (NQR) in superconducting specimens with $0.25 < x < 0.35$ display significant antiferromagnetic fluctuations at $T > T_C$ [208, 209]. These observations are especially important in the case of $Na_xCoO_2 \cdot yH_2O$ because precisely the spin fluctuations can fill the role of the possible mechanism of Cooper pairing in quasi-two-dimensional oxide compounds of transition metals.

Another enigmatic observation is that a long-range order forms only in a narrow range of concentrations ($0.75 < x < 0.9$). In fact, according to first-principle LDA calculations [210, 211], the ferromagnetic ground state is expected to form in a wide range of concentrations, from $x = 0.3$ to $x = 0.7$. Experimental data contradict this prediction. Several theories have been proposed to explain the observed behavior of magnetic ordering. The theory based on metallic behavior of layered cobaltites at practically any concentration considers the behavior of the magnetic susceptibility of collectivized electrons $\chi(q, \omega)$ [184, 212, 213]. It was also discovered that the peaks on $\chi(q, \omega)$ due to nesting of the Fermi surface depend critically on the level of doping. Indeed, if the doping level is low, the main contribution comes from scattering on the large Fermi pocket formed mostly by the a_{1g} band. This contribution stemming from the nesting vector of the 120-degree antiferromagnetism, $\mathbf{Q}_{AFM} = \{(2\pi/3, 2\pi/\sqrt{3}), (4\pi/3, 0)\}$, shows that the electron subsystem tends to this AFM order. Hence, if this order fails to form, AFM fluctuations should be observed; this conclusion agrees with experimental data. This tendency persists at concentrations up to a critical value x_c that depends on the deviation from the nesting condition due to the change in the volume of the Fermi surface, and also on the following factor. Band calculations produce a local minimum in the dispersion of the a_{1g} band in the neighborhood of the Γ point. In the case of doping with electrons, the a_{1g} band is filled and the local minimum causes the formation of a small-radius electron pocket. Scattering on the pocket begins to dominate and the system shows a tendency to ferromagnetic fluctuations at $x > x_c$. The concentration x_c obtained by band calculations with the model of nonzero-dispersion t_{2g} bands is equal to 0.58 [212]. An analysis of strong electron correlations in the Gutzwiller and Hubbard-I approximations showed that taking them into account does not result in qualitative changes, although x_c shifts to the range of large concentrations and increases to about 0.7 [184], which agrees well with observational data [159, 161, 207]. It is worth noting that ARPES techniques have failed to detect a small-radius electron pocket close to the Γ point; but as mentioned above, the modern ARPES data for layered cobaltites cannot be considered reliable because of the sensitivity of this method to the state of the surface of the specimen and also in view of the contradiction between the conclusions from the ARPES data and the experimental results produced by other methods.

Simultaneously taking electron correlations and the potential created by Na ions into account led to a similar value for x_c [214]. We note that the presence of a small-radius electron pocket was not a necessary condition for the formation of ferromagnetic order; the leading role in it was played by the potential of disordered Na.

In addition to the theory of magnetism of collectivized electrons, an approach exists based on the analogy to manganites and three-dimensional $LaCoO_3$ cobaltites. A scenario for the creation of a magnetic polaron leading to ferromagnetic fluctuations at high doping concentrations was studied in [215]. This scenario is based on the possibility of realizing an HS state in CoO_6 octahedra, which is in fact rather improbable in the case of this specific layered cobaltite because of the large splitting of the t_{2g} and e_g levels (~ 2 eV) and the relative smallness of the Hund exchange (~ 1 eV). All this leads to the energy of the HS state lying higher than that of the LS state by 1.75 eV [216], and hence to stabilization of the low-spin state as the ground state at any Na concentration. However, in subsequent paper [217], a hypothesis was advanced that even in the case of realization of the LS state as the ground level, the dynamic IS and HS states can affect the magnetic properties of quasiparticles.

Another interesting question is related to the ratio of in-plane and interplane exchange interactions. An analysis of neutron scattering data in [162–165] revealed that $J_{ab} = -6$ meV and $J_c = 12$ meV. This result seems at first glance to contradict the one expected for a quasi-two-dimensional system. But as was shown in [218], magnetic interaction along the c axis is enhanced owing to the presence of Na orbitals. Therefore, the magnetic properties of Na_xCoO_2 remain essentially three-dimensional despite its two-dimensional electron structure. It is interesting to note that the three-dimensionality of the properties is violated

when H_2O layers are added; this leads to two-dimensional magnetic fluctuations.

An additional factor causing suppression of the in-plane magnetic moment may be the frustration effect. Indeed, the planar lattice of Co ions is triangular. In this case of the AFM interaction with the nearest neighbors and magnetic Ising anisotropy, the long-range AFM order is suppressed. As a result, ordering is dictated by the FM interaction between next-to-nearest neighbors. Correspondingly, the exchange integral obtained from the analysis of neutron scattering in the ordered phase is in-plane ferromagnetic. At the same time, AFM fluctuations start playing a decisive role in the disordered phase because of the exchange between nearest neighbors. This situation is typical of a broad class of magnetically frustrated systems, which includes both oxides of transition metals and intermetallic compounds.

As regards the superconductivity of $Na_xCoO_2 \cdot yH_2O$, general agreement was not reached for a long time concerning the symmetry of the superconducting gap $\Delta_{\mathbf{k}}$. Studies of specific heat [219–222] and measurements of the penetration depth using muon spectroscopy (μSR) [223] revealed lines of zeros of $\Delta_{\mathbf{k}}$ on the Fermi surface. The same conclusion was obtained from the NMR measurement data on the spin–lattice relaxation [the quantity $1/(T_1T)$, where T_1 is the spin–lattice relaxation time] which yielded a power-law temperature dependence and no Hebel–Slichter peak so typical of the s-type superconductors [208, 209, 221, 224, 225]. At the same time, strong AFM fluctuations were observed at $T > T_c$. Early work devoted to studying the Knight shift as a function of temperature supported the choice of a spin-triplet symmetry of the superconducting gap because the Knight shift in the direction perpendicular to CoO_2 layers was practically independent of the temperature [226, 227]. This behavior of the Knight shift stimulated a series of theoretical papers treating the triplet superconductivity in $Na_xCoO_2 \cdot yH_2O$ [171, 180, 228–231]. However, modern high-precision NMR data [232, 233] detected a decrease in the Knight shift in all directions with decreasing the temperature, which is an unambiguous indication of the spin-singlet Cooper pairing.

The group-theory analysis classifies the symmetry of the singlet order parameter on the triangular lattice as follows:

- s-type, $\Delta_{\mathbf{k}} = \Delta_0$;
- extended s-type,
  $\Delta_{\mathbf{k}} = 2/3\,\Delta_0\left[\cos k_y + 2\cos\left(k_x\sqrt{3}/2\right)\cos\left(k_y/2\right)\right]$;
- $d_{x^2-y^2}$-type,
  $\Delta_{\mathbf{k}} = \Delta_0\left[\cos k_y - \cos\left(k_x\sqrt{3}/2\right)\cos\left(k_y/2\right)\right]$;
- d_{xy}-type, $\Delta_{\mathbf{k}} = \Delta_0\left[\sqrt{3}\,\sin\left(k_x\sqrt{3}/2\right)\sin\left(k_y/2\right)\right]$;
- $d_{x^2-y^2} + id_{xy}$-type

and higher harmonics (see [234] and the references therein). Both types of symmetry, $d_{x^2-y^2}$ and d_{xy}, are characterized by the presence of lines of zeros of $\Delta_{\mathbf{k}}$ on the Fermi surface. We note that the symmetry type $d_{x^2-y^2} + id_{xy}$ is then broken with respect to time reversal.

The effect of symmetry of the superconducting gap and electron structure on the dynamic spin susceptibility of the compound $Na_xCoO_2 \cdot yH_2O$ was systematically investigated in theoretical paper [235], where three models were studied: a single-band a_{1g} model with hopping between nearest neighbors, and a realistic three-band t_{2g} model, both with e_g' pockets on the Fermi surface and without them. It was possible to show that antiferromagnetic spin fluctuations with large wave vectors are responsible for the dominant contribution to the magnetic response in the normal state and that the presence or absence of e_g' pockets does not play a significant role. According to [235], the available set of experimental data indicates that the order parameter in the superconducting state must have the symmetry type $d_{x^2-y^2}$ or d_{xy}, while the symmetry $d_{x^2-y^2} + id_{xy}$ must be excluded.

A comparative analysis of superconductivity in HTSC cuprates and layered cobaltites seems to support the spin-fluctuation mechanism of Cooper pairing by exchanging two-dimensional AFM fluctuations in the two systems; this easily explains the d-type symmetry of the order parameter. We note that the difference between T_c values is determined in this scenario by the difference between exchange levels in cuprates and cobaltites. The role of water in cobaltites consists in the mutual repulsion of CoO_2 planes, which results in essentially two-dimensional magnetic fluctuations, similar to those found in HTSC. However, the role of the electron–phonon interaction, which is known to be important in cuprates (see [236] and [237]), must also be clarified in order to fully understand the nature of superconductivity in the two systems. For Na_xCoO_2, the strength of the electron–phonon interaction was derived by analyzing Raman scattering spectra as a function of doping concentration [238]. Even though the obtained value of T_c due to the electron–phonon interaction is near the experimental value, it remains unknown why in this case superconductivity sets in only after the intercalation of water and in a narrow range of doping concentrations.

5. Possible practical applications of cobaltites

Cobalt oxides are of enormous interest owing to the potential of their practical applications, which are evolving in several directions embracing solid-state power supply units [239–245], oxygen membranes [246, 247], catalyst systems [248, 249], membrane reactors for oxidizing hydrocarbons [250], gas sensors [251, 252], and thermoelectric devices [253, 254].

Most of the practical applications of these materials, with the exception of thermoelectric ones, are based on properties such as high electron and ion conductivities [246, 247, 255] and catalyst activities. The high ion conductivity is in turn related to the defect structure of these materials, mostly oxygen nonstoichiometry. The ion diffusion coefficient in cobaltites is greater than in manganates by several orders of magnitude [256, 257], which certainly creates better prerequisites for gas transport.

One of the first and currently best developed applications of cobalt oxides is their use as cathodes for solid oxide fuel cells (SOFCs). This kind of power supply has recently attracted much attention. Their advantage lies in their being highly efficient, being ecologically clean, and allowing miniaturization. A SOFC generates energy from substances such as hydrogen, carbon monoxide, and methanol [258]. It comprises an electrolyte and two electrodes. Oxidation of fuel at the anode releases electrons, which reach the cathode through an external circuit. The working electrode of a solid-state battery acts simultaneously as a charge source and a catalyst. Therefore, SOFC working principles can also be applied to electrocatalytic reactors, as was implemented in [259] for oxidation of methane.

The catalytic ability of cobalt oxides allows using them for oxidation of light volatile hydrocarbons. Catalytic oxidation is very important because it may proceed at sufficiently low temperatures. Noble metals are good catalysts, but they are very costly. The catalytic activity of perovskites is usually lower than that of noble metals [260]. But investigations have shown that practically the same results can be achieved with ceramic perovskites because of their porous structure and correspondingly higher area per unit volume [261]. Moreover, using the method of electrochemical catalysis borrowed from the SOFC technology greatly enhances the catalytic activity and allows obtaining products of chemical reactions in a reversible and controlled manner.

When cobalt oxides are used as SOFC cathodes or electrochemical catalysts and membranes, a very important stage is the passing of oxygen through a polycrystalline specimen. The gas transport through porous membranes includes surface reactions involving the transformation of oxygen in the lattice from molecular to ionic form. The main contribution to oxygen transport through ceramics comes from the oxygen diffusion across grain boundaries, and therefore the grain size and the technology of membrane manufacturing become very important. The thermodynamics of processes occurring at the so-called three-phase boundaries was treated in [262] in the case of ionic conductors; in fact, the rules used in developing specific devices are typically rather empirical. For example, it was established that high ionic conductivity is a signature of a cubic or rhombic structure [263], while thermodynamic stability increases with increasing the Goldschmidt number and ionic radius of the rare-earth cation [264]. The ionic conductivity and membrane permeability decrease with decreasing the ion radius. Knowing these correlations helps specify the doping strategy.

Great efforts have been devoted in recent decades to enhancing the efficiency and service life of solid-state electrochemical devices. It has proved possible to design devices up to 100 kW in power. Nonetheless, there are a number of problems connected with choosing materials for SOFC devices, mostly because of the high working temperature ($\sim 1000\,^{\circ}\mathrm{C}$). Such temperatures are required for achieving high ionic conductivity and sustaining sufficiently high rates of chemical reactions. Unfortunately, high operational temperatures entail a number of negative consequences. First, cyclic heating and cooling lead to material degradation. The exposure of ceramics to cyclic thermal loads of SOFC may result in mechanical stresses in them and mechanical failure. Second, even though cobalt oxides have a much higher conductivity than, for instance, $La_{1-x}Sr_xMnO_3$, their thermal stability is not as high as that of manganites, because high ionic conductivity implies weak interionic bonds, which are also responsible for the chemical composition. Finally, the third factor is that thermal expansion of cobaltites is typically considerable; this generates problems when combining different parts of a device, especially at high temperatures. A certain shortcoming of cobalt oxide cathodes is the impossibility of using them in combination with the traditional zirconium-based electrolyte, because chemical reactions in a heated system rapidly produce $La_2Zr_2O_7$ and $SrZrO_3$ dielectric phases [265]. However, a combination of cobaltites and electrolytes based on bismuth and cerium oxides looks quite promising [266].

Several approaches to overcoming these problems exist. The first approach is related to searching for new materials that combine high electron and ion conductivity and at the same time are compatible with other elements of the battery. In [267], materials such as $Ln_{0.4}Sr_{0.6}Co_{0.8}Fe_{0.2}O_{3-\delta}$ (Ln = La, Pr, Nd, Sm, Gd) and in [268], $Sm_{0.5}Sr_{0.5}CoO_3$ were studied with a view to using them as SOFC cathodes. The properties of $SrCoO_3$ were studied in [269]. Perhaps the best result is to be obtained by using $A_2B_2O_5$-based compounds, such as $Sr_{0.9}Ce_{0.1}Co_{0.3}Fe_{0.7}O_{2.5-\delta}$ [270], $Sr_{0.9}La_{0.1}Co_{0.3}Fe_{0.7}O_{2.5-\delta}$ [246], and compositions with excess oxygen content, such as $Pr_2(Ni, Co)O_{4+\delta}$ [271]. Layered La_2CoO_4 and $La_{2_x}Sr_xCoO_4$ compounds [272, 273] demonstrate an unusually high rate of oxygen transport. The high catalytic activity of these materials with respect to CO and C_3H_8 was established. Cobalt oxides with the structure K_2NiF_4 have not yet been sufficiently studied, but a hypothesis was formulated in [274] that the use of precisely these materials may allow decreasing the working temperature to room temperature.

The second approach consists in developing multilayer systems. It is well known that the quality of contact between two materials having different physical properties can be improved by a gradual change in composition in the region of contact [275]. The composition of each individual layer in this region is adjusted such that one composition smoothly transforms into another.

Another important application of cobalt oxides is using them as materials for gas sensors. Such sensors are required in control devices for chemical processes and for monitoring the state of the environment; they are also used for medical purposes. For example, it is important in many cases to measure the concentration of ammonia, NH_3. The existing sensors determining the concentration of ammonia already use semiconducting materials, organic compounds, and carbon nanotubes [276–278]. But the sensitivity of all these devices is low and their practical applications are significantly limited. A special problem is their low selectivity: many devices sensitive to NH_3 are at the same time highly sensitive to other natural gases. In [250], the high catalytic activity of polycrystalline $LaCoO_3$ was used to develop a converter that oxidizes ammonia to NO_x rapidly and efficiently. The amount of NO_x produced can be determined, as shown in [250], with high accuracy by the chemiluminescence technique, which has high sensitivity and good selectivity. In [279], another principle of measuring the partial pressure was used — thermogravimetric analysis based on measuring the changes in the weight of a membrane made of $La_{1-x}Sr_xCo_{1-y}Fe_yO_{3-\delta}$ as a result of desorption or adsorption of oxygen. The high sensitivity of the method has been confirmed. $Gd_{0.7}Ca_{0.3}CoO_{3-\delta}$ can also be used as a gas sensor [280].

An interesting and important development is outlined in [281], where it was discovered that the mixed compound $Sr_xCa_{1-x}Fe_{0.5}Co_{0.5}O_{3-\delta}$ has a high adsorption capacity with respect to carbon dioxide; this is especially important for counteracting the greenhouse effect.

The bibliography given below of the already implemented applications of cobalt oxides, as well as those expected to be implemented, based on their transport and chemical properties, is far from complete, but it is already clear that considerable progress has been achieved in this applied field. As regards the utilization of the unusual and strongly pronounced thermoelectric properties of cobaltites, this is still a matter for the future. Nevertheless, we can cite paper [253] as an example of an already completed development: a thin-film thermocouple is described, based on

$La_{1-x}Sr_xCoO_3$, fabricated by laser sputtering onto a sapphire substrate. Good stability of the composition was observed at temperatures up to 1273 K, especially at $x = 0.3$. Electric conductivity and the Seebeck coefficient were stable up to $T = 1023$ K. This thermoelectric device can therefore be successfully used for measuring high temperatures.

6. Conclusion

We hope that the example of several families of cobalt oxide compounds has allowed us, at least partly, to demonstrate the variety of physical properties revealed by these compounds and to show how these properties are formed under the interacting influences of various — lattice, charge, spin, and orbital — degrees of freedom. Despite impressive progress achieved in the physics of cobaltites, many issues remain open or without a final solution, including the widely known problem of the instability of the spin state of cobalt ions, or the determination of the nature of superconductivity and magnetism in $Na_xCoO_2 \cdot yH_2O$. This is meant to show that cobalt oxide compounds offer a broad range of problems for physicists, both in fundamental and in applied research.

This work was financially supported by the RFBR (projects 09-02-00171-a, 07-02-00226, and 09-02-00127), the Federal Agency of Science and Innovation (grant MK-4278.2008.2), and the Presidium of the Russian Academy of Sciences Program No. 5, Quantum Physics of Condensed Media (project No. 7). I.M.E.'s work was supported by the program for Leading Science Schools of the Ministry of Education and Science of the Russian Federation (grant 2.1.1/3199).

References

1. Maekawa S et al. *Physics of Transition Metal Oxides* (Berlin: Springer, 2004)
2. Maksimov E G *Usp. Fiz. Nauk* **170** 1033 (2000) [*Phys. Usp.* **43** 965 (2000)]
3. Sadovskiĭ M V *Usp. Fiz. Nauk* **171** 539 (2001) [*Phys. Usp.* **44** 515 (2001)]
4. Belyavskii V I, Kopaev Yu V *Usp. Fiz. Nauk* **176** 457 (2006) [*Phys. Usp.* **49** 441 (2006)]
5. Damascelli A, Hussain Z, Shen Z-X *Rev. Mod. Phys.* **75** 473 (2003)
6. Tokura Y (Ed.) *Colossal Magnetoresistive Oxides* (Amsterdam: Gordon and Breach, 2000)
7. Izyumov Yu A, Skryabin Yu N *Usp. Fiz. Nauk* **171** 121 (2001) [*Phys. Usp.* **44** 109 (2001)]
8. Kagan M Yu, Kugel' K I *Usp. Fiz. Nauk* **171** 577 (2001) [*Phys. Usp.* **44** 553 (2001)]
9. Dagotto E *Nanoscale Phase Separation and Colossal Magnetoresistance* (Berlin: Springer, 2003)
10. Mackenzie A P, Maeno Y *Rev. Mod. Phys.* **75** 657 (2003)
11. Ovchinnikov S G *Usp. Fiz. Nauk* **173** 27 (2003) [*Phys. Usp.* **46** 21 (2003)]
12. Takada K et al. *Nature* **422** 53 (2003)
13. Briceño G et al. *Science* **270** 273 (1995)
14. Maignan A et al. *J. Solid State Chem.* **142** 247 (1999)
15. Jirák Z et al. *Phys. Rev. B* **78** 014432 (2008)
16. Taskin A A, Lavrov A N, Ando Y *Phys. Rev. B* **73** 121101(R) (2006)
17. Szymczak H *J. Magn. Magn. Mater.* **200** 425 (1999)
18. Ovchinnikov S G *Usp. Fiz. Nauk* **169** 869 (1999) [*Phys. Usp.* **42** 779 (1999)]
19. Demazeau G, Pouchard M, Hagenmuller P *J. Solid State Chem.* **9** 202 (1974)
20. Medarde M L *J. Phys. Condens. Matter* **9** 1679 (1997)
21. Chang C Y et al. *Chinese J. Phys.* **41** 662 (2003)
22. Knížek K et al. *Eur. Phys. J. B* **47** 213 (2005)
23. Berggold K et al. *Phys. Rev. B* **78** 134402 (2008)
24. Bhide V G et al. *Phys. Rev. B* **6** 1021 (1972)
25. Zobel C et al. *Phys. Rev. B* **66** 020402 (2002)
26. Asai K et al. *Phys. Rev. B* **40** 10982 (1989)
27. Itoh M et al. *J. Phys. Soc. Jpn.* **64** 3967 (1995)
28. Itoh M et al. *Physica B* **259 – 261** 902 (1999)
29. Itoh M et al. *Physica B* **281 – 282** 510 (2000)
30. Im Y S et al. *J. Phys. Chem. Solids* **58** 2079 (1997)
31. Tachibana M et al. *Phys. Rev. B* **77** 094402 (2008)
32. Vankó G et al. *Phys. Rev. B* **73** 024424 (2006)
33. Lengsdorf R et al. *Phys. Rev. B* **69** 140403 (2004)
34. Boukheddaden K et al. *Phys. Rev. B* **62** 14806 (2000)
35. Sudheendra L et al. *Ferroelectrics* **306** 227 (2004)
36. Haverkort M W et al. *Phys. Rev. Lett.* **97** 176405 (2006)
37. Tokura Y et al. *Phys. Rev. B* **58** R1699 (1998)
38. Thornton G et al. *J. Phys. C* **21** 2871 (1988)
39. Ivanova N B et al. *Fiz. Tverd. Tela* **49** 1427 (2007) [*Phys. Solid State* **49** 1498 (2007)]
40. Vogt T et al. *Phys. Rev. Lett.* **84** 2969 (2000)
41. Raccah P M, Goodenough J B *Phys. Rev.* **155** 932 (1967)
42. Thornton G, Owen I W, Diakun G P *J. Phys. Condens. Matter* **3** 417 (1991)
43. Korotin M A et al. *Phys. Rev. B* **54** 5309 (1996)
44. Tanabe Y, Sugano S *J. Phys. Soc. Jpn.* **9** 766 (1954)
45. Ropka Z, Radwanski R J *Physica B* **312 – 313** 777 (2002)
46. Goodenough J B *J. Phys. Chem. Solids* **6** 287 (1958)
47. Blasse G *J. Appl. Phys.* **36** 879 (1965)
48. Jonker G H *J. Appl. Phys.* **37** 1424 (1966)
49. Bhide V G et al. *Phys. Rev. B* **6** 1021 (1972)
50. Khomskii D I, Löw U *Phys. Rev. B* **69** 184401 (2004)
51. Doumerc J-P et al. *J. Solid State Chem.* **147** 211 (1999)
52. Doumerc J-P et al. *J. Mater. Chem.* **11** 78 (2001)
53. Potze R H, Sawatzky G A, Abbate M *Phys. Rev. B* **51** 11501 (1995)
54. Saitoh T et al. *Phys. Rev. B* **55** 4257 (1997)
55. Yamaguchi S et al. *Phys. Rev. B* **53** R2926 (1996)
56. Abbate M et al. *Phys. Rev. B* **47** 16124 (1993)
57. Asai K et al. *J. Phys. Soc. Jpn.* **67** 290 (1998)
58. Stølen S et al. *Phys. Rev. B* **55** 14103 (1997)
59. Klie R F et al. *Phys. Rev. Lett.* **99** 047203 (2007)
60. Maris G et al. *Phys. Rev. B* **67** 224423 (2003)
61. Phelan D, Yu J, Louca D *Phys. Rev. B* **78** 094108 (2008)
62. Sundaram N et al. *Phys. Rev. Lett.* **102** 026401 (2009)
63. Noguchi S et al. *Phys. Rev. B* **66** 094404 (2002)
64. Medarde M et al. *Phys. Rev. B* **73** 054424 (2006)
65. Pandey S K et al. *Phys. Rev. B* **77** 045123 (2008)
66. Pandey S K et al. *Phys. Rev. B* **77** 115137 (2008)
67. Radwański R J, Ropka Z *Physica B* **281 – 282** 507 (2000)
68. Ropka Z, Radwanski R J *Phys. Rev. B* **67** 172401 (2003)
69. Tanaka A, Jo T *J. Phys. Soc. Jpn.* **63** 2788 (1994)
70. de Groot F M F *J. Electron Spectrosc. Relat. Phenom.* **67** 529 (1994)
71. Thole B T et al. *Phys. Rev. Lett.* **68** 1943 (1992)
72. Saitoh T et al. *Phys. Rev. B* **52** 7934 (1995)
73. Burnus T et al. *Phys. Rev. B* **74** 245111 (2006)
74. Nekrasov I A et al. *Phys. Rev. B* **68** 235113 (2003)
75. Ovchinnikov S G, Orlov Yu S *Zh. Eksp. Teor. Fiz.* **131** 485 (2007) [*JETP* **104** 436 (2007)]
76. Craco L, Müller-Hartmann E *Phys. Rev. B* **77** 045130 (2008)
77. Phelan D et al. *Phys. Rev. Lett.* **96** 027201 (2006)
78. Louca D *J. Supercond.: Incorp. Novel Magn.* **15** 591 (2002)
79. Baier J et al. *Phys. Rev. B* **71** 014443 (2005)
80. Berggold K et al. *Phys. Rev. B* **72** 155116 (2005)
81. Loshkareva N N et al. *J. Magn. Magn. Mater.* **258 – 259** 277 (2003)
82. Tang Y, Sun Y, Cheng Z *Phys. Rev. B* **73** 012409 (2006)
83. Wu J et al. *Phys. Rev. B* **73** 020404(R) (2006)
84. Podlesnyak A et al. *Phys. Rev. Lett.* **101** 247603 (2008)
85. Kazak N V et al. *J. Magn. Magn. Mater.* **321** 1266 (2009)
86. Taskin A A, Lavrov A N, Ando Y *Phys. Rev. Lett.* **90** 227201 (2003)
87. Kobayashi W et al. *Phys. Rev. B* **72** 104408 (2005)
88. Morimoto Y et al. *Phys. Rev. B* **58** R13334 (1998)
89. Awana V P S et al. *J. Magn. Magn. Mater.* **250** 6 (2002)
90. Señarís-Rodríguez M A, Goodenough J B *J. Solid State Chem.* **118** 323 (1995)
91. Bocquet A E et al. *Phys. Rev. B* **46** 3771 (1992)
92. Mizokawa T et al. *Phys. Rev. B* **49** 7193 (1994)
93. van Elp J et al. *Phys. Rev. B* **45** 1612 (1992)

94. Jirák Z et al. *Phys. Rev. B* **78** 014432 (2008)
95. Kuhns P L et al. *Phys. Rev. Lett.* **91** 127202 (2003)
96. Nagaev E L *Fizika Magnitnykh Poluprovodnikov* (Physics of Magnetic Semiconductors) (Moscow: Nauka, 1979) [Translated into English (Moscow: Mir Publ., 1983)]
97. Troyanchuk I O et al. *Phys. Rev. B* **58** 2418 (1998)
98. Tranquada J M et al. *Nature* **375** 561 (1995)
99. Morimoto Y et al. *Phys. Rev. B* **56** 14879 (1997)
100. Streule S et al. *Phys. Rev. B* **73** 024423 (2006)
101. Kundu A et al. *J. Solid State Chem.* **180** 1318 (2007)
102. Zhou Sh et al. *Phys. Rev. B* **76** 172407 (2007)
103. Fuchs D et al. *Phys. Rev. B* **75** 144402 (2007)
104. Androulakis J, Katsarakis N, Giapintzakis J *Phys. Rev. B* **64** 174401 (2001)
105. Harada A et al. *Phys. Rev. B* **75** 184426 (2007)
106. Yan J-Q, Zhou J-S, Goodenough J B *Phys. Rev. B* **70** 014402 (2004)
107. Giblin S R et al. *Europhys. Lett.* **70** 677 (2005)
108. Pinta C et al. *Phys. Rev. B* **78** 174402 (2008)
109. Fita I et al. *Phys. Rev. B* **77** 224421 (2008)
110. Lourerio S M et al. *Chem. Mater.* **12** 3181 (2000)
111. Yamaura K, Huang Q, Cava R J *J. Solid State Chem.* **146** 277 (1999)
112. Yamaura K, Young D P, Cava R J *Phys. Rev. B* **63** 064401 (2001)
113. Matsuno J et al. *Phys. Rev. Lett.* **93** 167202 (2004)
114. Wu H *J. Phys. Condens. Matter* **15** 503 (2003)
115. Vogt T et al. *Phys. Rev. Lett.* **84** 2969 (2000)
116. Khalyavin D D *Phys. Rev. B* **72** 134408 (2005)
117. Zhitlukhina E S et al. *Fiz. Nizk. Temp.* **31** 1266 (2005) [*Low Temp. Phys.* **31** 963 (2005)]
118. Hu Z et al. *Phys. Rev. Lett.* **92** 207402 (2004); cond-mat/0310138
119. Pardo V, Bladomir D *Phys. Rev. B* **73** 165117 (2006)
120. Fauth F et al. *Eur. Phys. J. B* **21** 163 (2001)
121. Fauth F et al. *Phys. Rev. B* **66** 184421 (2002)
122. Morimoto Y et al. *Phys. Rev. B* **61** R13325 (2000)
123. Frontera C et al. *Phys. Rev. B* **65** 180405 (2002)
124. Akahoshi D, Ueda Y *J. Solid State Chem.* **156** 355 (2001)
125. Baran M et al. *J. Phys. Condens. Matter* **17** 5613 (2005)
126. Gatalskaya V I et al. *Fiz. Tverd. Tela* **49** 102 (2007) [*Phys. Solid State* **49** 107 (2007)]
127. Podlesnyak A et al. *Physica B* **378 – 380** 537 (2006)
128. Khalyavin D D et al. *Phys. Rev. B* **75** 134407 (2007)
129. Taskin A A, Lavrov A N, Ando Y *Phys. Rev. B* **71** 134414 (2005)
130. Luetkens H et al. *Phys. Rev. Lett.* **101** 017601 (2008)
131. Maignan A et al. *Phys. Rev. Lett.* **93** 026401 (2004)
132. Taskin A A, Ando Y *Phys. Rev. Lett.* **95** 176603 (2005)
133. Terasaki I, Sasago Y, Uchinokura K *Phys. Rev. B* **56** R12685 (1997)
134. Gardner J S, Paul D McK, Lcbech B *Physica B* **234 – 236** 721 (1997)
135. Ravindran P et al. *Phys. Rev. B* **60** 16423 (1999)
136. Chainani A, Mathew M, Sarma D D *Phys. Rev. B* **46** 9976 (1992)
137. Mahendiran R et al. *J. Phys. Condens. Matter* **7** L561 (1999)
138. Zhuang M et al. *Phys. Lett. A* **255** 354 (1999)
139. Furukawa Y, Wada S, Yamada Y *J. Phys. Soc. Jpn.* **62** 1127 (1993)
140. Morimoto Y et al. *Phys. Rev. B* **55** R14725 (1997)
141. Demazeau G et al. *Nouveau J. Chim.* **3** 171 (1979)
142. Morimoto Y, Arima T, Tokura Y *J. Phys. Soc. Jpn.* **64** 4117 (1995)
143. Wang J et al. *J. Phys. Condens. Matter* **12** 7425 (2000)
144. Maignan A et al. *Eur. Phys. J. B* **15** 657 (2000)
145. Hardy V et al. *Phys. Rev. B* **68** 014424 (2003)
146. Aasland S, Fjellvåg H, Hauback B *Solid State Commun.* **101** 187 (1997)
147. Kageyama H et al. *J. Phys. Soc. Jpn.* **66** 1607 (1997)
148. Flahaut D et al. *Phys. Rev. B* **70** 094418 (2004)
149. Sangregorio C et al. *Phys. Rev. Lett.* **78** 4645 (1997)
150. Agrestini S et al. *Phys. Rev. Lett.* **101** 097207 (2008)
151. Vidya R et al. *Phys. Rev. Lett.* **91** 186404 (2003)
152. Sampathkumaran E V et al. *Phys. Rev. B* **70** 014437 (2004)
153. Eyert V et al. *Chem. Phys. Lett.* **385** 249 (2004)
154. Whangbo M-H et al. *Solid State Commun.* **125** 413 (2003)
155. Dai D, Whangbo M-H *Inorg. Chem.* **44** 4407 (2005)
156. Wu H et al. *Phys. Rev. Lett.* **95** 186401 (2005)
157. Schaak R E et al. *Nature* **424** 527 (2003)
158. Jorgensen J D et al. *Phys. Rev. B* **68** 214517 (2003)
159. Foo M L et al. *Phys. Rev. Lett.* **92** 247001 (2004)
160. Jin R et al. *Phys. Rev. Lett.* **91** 217001 (2003)
161. Motohashi T et al. *Phys. Rev. B* **67** 064406 (2003)
162. Boothroyd A T et al. *Phys. Rev. Lett.* **92** 197201 (2004)
163. Bayrakci S P et al. *Phys. Rev. Lett.* **94** 157205 (2005)
164. Helme L M et al. *Phys. Rev. Lett.* **94** 157206 (2005)
165. Bayrakci S P et al. *Phys. Rev. B* **69** 100410 (2004)
166. Kawata T et al. *Phys. Rev. B* **60** 10584 (1999)
167. Bañobre-López M et al. *Chem. Mater.* **17** 1965 (2005)
168. Lee M et al. *Nature Mater.* **5** 537 (2006)
169. Wang Y et al. *Nature* **423** 425 (2003)
170. Lee K-W, Kuneš J, Pickett W E *Phys. Rev. B* **70** 045104 (2004)
171. Johannes M D et al. *Phys. Rev. Lett.* **93** 097005 (2004)
172. Johannes M D, Singh D J *Phys. Rev. B* **70** 014507 (2004)
173. Hasan M Z et al. *Phys. Rev. Lett.* **92** 246402 (2004)
174. Yang H-B et al. *Phys. Rev. Lett.* **92** 246403 (2004)
175. Yang H-B et al. *Phys. Rev. Lett.* **95** 146401 (2005)
176. Qian D et al. *Phys. Rev. Lett.* **96** 216405 (2006)
177. Qian D et al. *Phys. Rev. Lett.* **97** 186405 (2006)
178. Shimojima T et al. *Phys. Rev. Lett.* **97** 267003 (2006)
179. Geck J et al. *Phys. Rev. Lett.* **99** 046403 (2007)
180. Kuroki K, Tanaka Y, Arita R *Phys. Rev. Lett.* **93** 077001 (2004)
181. Mochizuki M, Yanase Y, Ogata M *Phys. Rev. Lett.* **94** 147005 (2005)
182. Zhang P et al. *Phys. Rev. Lett.* **93** 236402 (2004)
183. Zhou S et al. *Phys. Rev. Lett.* **94** 206401 (2005)
184. Korshunov M M et al. *Phys. Rev. B* **75** 094511 (2007)
185. Gutzwiller M C *Phys. Rev. Lett.* **10** 159 (1963)
186. Gutzwiller M C *Phys. Rev.* **134** A923 (1964)
187. Gutzwiller M C *Phys. Rev.* **137** A1726 (1965)
188. Bünemann J, Gebhard F, Weber W *J. Phys. Condens. Matter* **9** 7343 (1997)
189. Liebsch A, Ishida H *Eur. Phys. J. B* **61** 405 (2008)
190. Marianetti C A, Haule K, Parcollet O *Phys. Rev. Lett.* **99** 246404 (2007)
191. Ishida H, Johannes M D, Liebsch A *Phys. Rev. Lett.* **94** 196401 (2005)
192. Landron S, Lepetit M-B *Phys. Rev. B* **74** 184507 (2006)
193. Pillay D et al. *Phys. Rev. B* **78** 012501 (2008); arXiv:0804.3768
194. Balicas L et al. *Phys. Rev. Lett.* **97** 126401 (2006)
195. Balicas L et al. *Phys. Rev. Lett.* **94** 236402 (2005)
196. Jin R et al. *Phys. Rev. B* **72** 060512 (2005)
197. Yokoi M et al. *J. Phys. Soc. Jpn.* **74** 3046 (2005)
198. Oeschler N et al. *Phys. Rev. B* **78** 054528 (2008)
199. Laverock J et al. *Phys. Rev. B* **76** 052509 (2007)
200. Singh D J, Kasinathan D *Phys. Rev. Lett.* **97** 016404 (2006)
201. Huang Q et al. *J. Phys. Condens. Matter* **16** 5803 (2004)
202. Zandbergen H W et al. *Phys. Rev. B* **70** 024101 (2004)
203. Bobroff J et al. *Phys. Rev. Lett.* **96** 107201 (2006)
204. Argyriou D N et al. *Phys. Rev. B* **76** 134506 (2007)
205. Ning F L et al. *Phys. Rev. Lett.* **100** 086405 (2008); arXiv:0711.4023
206. Yokoi M et al., arXiv:0803.3255
207. Alloul H et al. *Europhys. Lett.* **82** 17002 (2008)
208. Fujimoto T et al. *Phys. Rev. Lett.* **92** 047004 (2004)
209. Zheng G et al. *J. Phys. Condens. Matter* **18** L63 (2006)
210. Singh D J *Phys. Rev. B* **68** 020503 (2003)
211. Singh D J *Phys. Rev. B* **61** 13397 (2000)
212. Korshunov M M et al. *Pis'ma Zh. Eksp. Teor. Fiz.* **84** 769 (2006) [*JETP Lett.* **84** 650 (2006)]
213. Kuroki K et al. *Phys. Rev. Lett.* **98** 136401 (2007)
214. Gao M, Zhou S, Wang Z *Phys. Rev. B* **76** 180402(R) (2007)
215. Daghofer M, Horsch P, Khaliullin G *Phys. Rev. Lett.* **96** 216404 (2006)
216. Shorikov A O, Anisimov V I, Korshunov M M, arXiv:0705.1408
217. Chaloupka J, Khaliullin G *Prog. Theor. Phys. Suppl.* (176) 50 (2008); arXiv:0806.1682
218. Johannes M D, Mazin I I, Singh D J *Phys. Rev. B* **71** 214410 (2005)
219. Cao G et al. *J. Phys. Condens. Matter* **15** L519 (2003)
220. Lorenz B et al. *Physica C* **402** 106 (2004)
221. Yang H D et al. *Phys. Rev. B* **71** 020504 (2005)
222. Jin R et al. *Phys. Rev. B* **72** 060512 (2005)
223. Kanigel A et al. *Phys. Rev. Lett.* **92** 257007 (2004)
224. Ishida K et al. *J. Phys. Soc. Jpn.* **72** 3041 (2003)
225. Michioka C et al. *J. Phys. Soc. Jpn.* **75** 063701 (2006)
226. Kato M et al. *Physica B* **359 – 361** 482 (2005)

227. Ihara Y et al. *J. Phys. Soc. Jpn.* **75** 013708 (2006)
228. Tanaka A, Hu X *Phys. Rev. Lett.* **91** 257006 (2003)
229. Motrunich O I, Lee P A *Phys. Rev. B* **70** 024514 (2004)
230. Kuroki K, Tanaka Y, Arita R *Phys. Rev. B* **71** 024506 (2005)
231. Mochizuki M, Yanase Y, Ogata M *Phys. Rev. Lett.* **94** 147005 (2005)
232. Zheng G et al. *Phys. Rev. B* **73** 180503(R) (2006)
233. Kobayashi Y et al. *J. Phys. Soc. Jpn.* **75** 074717 (2006)
234. Mazin I I, Johannes M D *Nature Phys.* **1** 91 (2005)
235. Korshunov M M, Eremin I *Phys. Rev. B* **77** 064510 (2008)
236. Maksimov E G, Dolgov O V *Usp. Fiz. Nauk* **177** 983 (2007) [*Phys. Usp.* **50** 933 (2007)]
237. Ovchinnikov S G, Shneider E I "Temperaturnyi izotop-effekt v VTSP kupratakh" ("Temperature isotope effect in HTSC cuprates"), in *Tret'ya Mezhdunar. Konf. "Fundamental'nye Problemy Vysokotemperaturnoi Sverkhprovodimosti" FPS-08, 13–17 Oktyabrya 2008 goda, g. Zvenigorod: Sbornik Tezisov* (Collected Papers of the Intern. Conf. on Fundamental Problems of High-Temperature Superconductivity, FP-08, 13–17 October 2008, Zvenigorod: Abstracts of Papers) (Moscow: FIAN, 2008) p. 44
238. Donkov A et al. *Phys. Rev. B* **77** 100504(R) (2008)
239. Tedmon C S (Jr.), Spacil H S, Mitoff S P *J. Electrochem. Soc.* **116** 1170 (1969)
240. Spinicci R et al. *J. Mol. Catal. A* **197** 147 (2003)
241. Drozhzhin O A, Chernov S V *Al'ternativnaya Energetika Ekologiya* (2) 99 (2008)
242. Steele B C H *Solid State Ionics* **134** 3 (2000)
243. Takeda Y et al. *Solid State Ionics* **86–88** 1187 (1996)
244. Lin H et al. *J. Solid State Electrochem.* **8** 450 (2004)
245. Wang P et al. *J. Alloys Compounds* **311** 53 (2000)
246. Teraoka Y et al. *Chem. Lett.* 1743 (1985)
247. Teraoka Y et al. *Mater. Res. Bull.* **23** 51 (1988)
248. Nakamura T, Misono M, Yoneda Y *Bull. Chem. Soc. Jpn.* **55** 394 (1982)
249. Arai H et al. *Appl. Catal.* **26** 265 (1986)
250. Shi J et al. *Talanta* **61** 157 (2003)
251. Yamamura Y, Ninomiya Y, Sekido S, in *Chemical Sensors: Proc. of the Intern. Meeting, Fukuoka, Japan, September 19–22, 1983* (Eds T Seiyama et al.) (Tokyo: Kodansha, 1983) p. 187
252. Michel C R et al. *Mater. Res. Bull.* **39** 2295 (2004)
253. Bhatt H D et al. *Thin Solid Films* **350** 249 (1999)
254. Moon J-W et al. *Mater. Lett.* **48** 225 (2001)
255. Mizusaki J et al. *J. Electrochem. Soc.* **136** 2082 (1989)
256. Steele B C H, Bae J-M *Solid State Ionics* **106** 255 (1998)
257. Lane J A et al. *Solid State Ionics* **121** 201 (1999)
258. Coccia L G et al. *Appl. Surf. Sci.* **96–98** 795 (1996)
259. Tsiakaras P et al. *Appl. Catal. A* **169** 249 (1998)
260. Spivey J J *Ind. Eng. Chem. Res.* **26** 2165 (1987)
261. Gaillard F et al. *Catal. Lett.* **96** 177 (2004)
262. Wiemhöfer H-D *Solid State Ionics* **75** 167 (1995)
263. Cook R L, Sammells A F *Solid State Ionics* **45** 311 (1991)
264. Yokokawa H et al. *Solid State Ionics* **52** 43 (1992)
265. McEvoy A J *Solid State Ionics* **132** 159 (2000)
266. Kharton V V, Naumovich E N, Samokhval V V *Solid State Ionics* **99** 269 (1997)
267. Tu H Y et al. *Solid State Ionics* **117** 277 (1999)
268. Xia C et al. *Solid State Ionics* **149** 11 (2002)
269. Ullmann H et al. *J. Eur. Ceramic Soc.* **19** 791 (1999)
270. Ullmann H, Trofimenko N *Solid State Ionics* **119** 1 (1999)
271. Pizzini S, in *Fast Ion Transpot in Solids. Solid State Batteries and Devices* (Ed. W van Gool) (Amsterdam: North-Holland, 1973) p. 461
272. Holtappels P, Bagger C *J. Eur. Ceramic Soc.* **22** 41 (2002)
273. Hart N T et al. *J. Rower Sources* **106** 42 (2002)
274. Marquis B T, Vetelino J F *Sens. Actuators B* **77** 100 (2001)
275. Gangopadhyay R, De A *Sens. Actuators B* **77** 326 (2001)
276. Davazoglou D, Dritsas T *Sens. Actuators B* **77** 359 (2001)
277. Zheng Y, Lin Y S *Solid State Ionics* **110** 209 (1998)
278. Nigge U et al. *Solid State Ionics* **146** 163 (2002)
279. Nemudry A, Rudolf P, Schöllhorn R *Solid State Ionics* **109** 213 (1998)
280. Yang X, Luo L, Zhong H *React. Kinet. Catal. Lett.* **81** 219 (2004)
281. Goldberg E et al. *Solid State Ionics* **110** 223 (1998)